Journal Pre-proof

IMM-H007 promotes hepatic cholesterol and triglyceride metabolism by activating AMPK*α* to attenuate hypercholesterolemia

Jiaqi Li, Mingchao Wang, Kai Qu, Yuyao Sun, Zequn Yin, Na Dong, Xin Sun, Yitong Xu, Liang Chen, Shuang Zhang, Xunde Xian, Suowen Xu, Likun Ma, Yajun Duan, Haibo Zhu

PII: S2211-3835(25)00319-3

DOI: https://doi.org/10.1016/j.apsb.2025.05.015

Reference: APSB 2390

To appear in: *Acta Pharmaceutica Sinica B*

Received Date: 25 December 2024

Revised Date: 26 January 2025

Accepted Date: 11 February 2025

Please cite this article as: Li J, Wang M, Qu K, Sun Y, Yin Z, Dong N, Sun X, Xu Y, Chen L, Zhang S, Xian X, Xu S, Ma L, Duan Y, Zhu H, IMM-H007 promotes hepatic cholesterol and triglyceride metabolism by activating AMPK*α* to attenuate hypercholesterolemia, *Acta Pharmaceutica Sinica B*, https://doi.org/10.1016/j.apsb.2025.05.015.

Original article

IMM-H007 promotes hepatic cholesterol and triglyceride metabolism by activating AMPK*α* to attenuate hypercholesterolemia

Jiaqi Li[a], Mingchao Wang[b], Kai Qu[b], Yuyao Sun[c,] Zequn Yin[a], Na Dong[a], Xin Sun[d], Yitong Xu[e], Liang Chen[f], Shuang Zhang[g], Xunde Xian[e], Suowen Xu[h i], Likun Ma[a], Yajun Duan[a,*], Haibo Zhu[b,*]

[a]*Department of Cardiology, the First Affiliated Hospital of USTC, Division of Life Sciences and Medicine, University of Science and Technology of China, Hefei 230001, China*

[b]*State Key Laboratory for Bioactive Substances and Functions of Natural Medicines, Beijing Key Laboratory of New Drug Mechanisms and Pharmacological Evaluation Study, Institute of Materia Medica, Chinese Academy of Medical Sciences and Peking Union Medical College, Beijing 100050, China*

[c]*College of Life Sciences, State Key Laboratory of Medicinal Chemical Biology, Key Laboratory of Bioactive Materials of Ministry of Education, Nankai University, Tianjin 300071, China*

[d]*State Key Laboratory of Common Mechanism Research for Major Diseases, Department of Biochemistry and Molecular Biology, Institute of Basic Medical Sciences, Chinese Academy of Medical Sciences and Peking Union Medical College, Beijing 100005, China*

[e]*Institute of Cardiovascular Sciences, State Key Laboratory of Vascular Homeostasis and Remodeling, School of Basic Medical Sciences, Peking University, Beijing 100083, China*

[f]*College of Life Science, Anhui Medical University, Hefei 230032, China*

[g]*Key Laboratory of Metabolism and Regulation for Major Diseases of Anhui Higher Education Institutes, College of Food and Biological Engineering, Hefei University of Technology, Hefei 230009, China*

[h]*Department of Endocrinology, the First Affiliated Hospital of USTC, Division of Life Sciences and Medicine, University of Science and Technology of China, Hefei 230001, China*

[i]*Anhui Provincial Key Laboratory of Metabolic Health and Panvascular Diseases, Hefei 23001, China*

Received 25 December 2024; received in revised form 26 January 2025; accepted 11 February 2025

*Corresponding authors.

E-mail addresses: zhuhaibo@imm.ac.cn (Haibo Zhu), yajunduan@ustc.edu.cn (Yajun Duan).

Running title: IMM-H007 reduces hypercholesterolemia and atherosclerosis

Graphical abstract

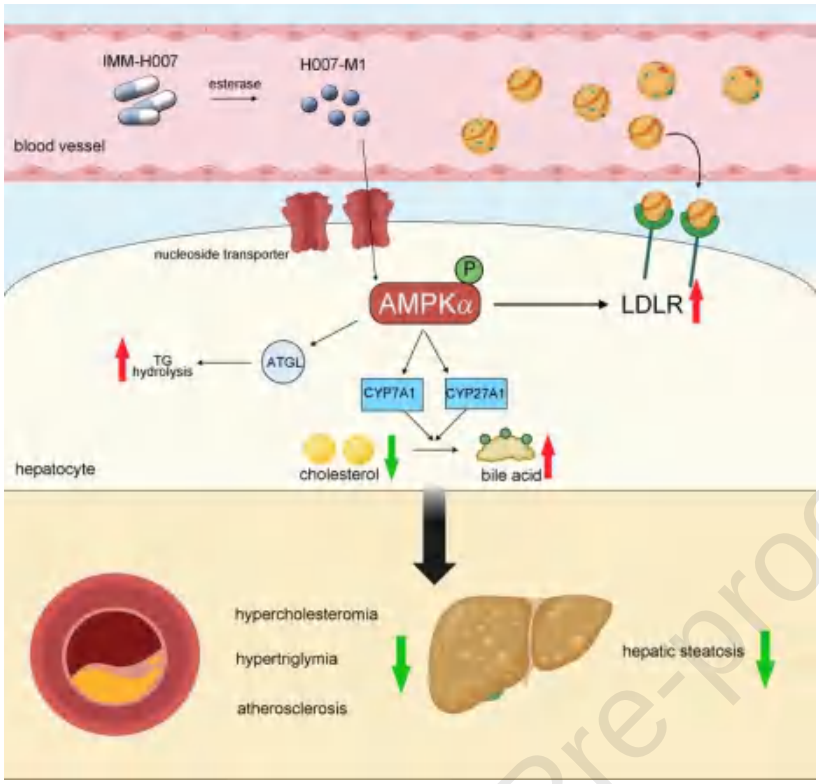

IMM-H007 hydrolyzes to H007-M1, activating hepatic AMPKα1/2 to promote cholesterol uptake by the liver, accelerating cholesterol conversion to bile acids, and improving triglyceride metabolism, thereby suppressing hypercholesterolemia and atherosclerosis.

Original article

IMM-H007 promotes hepatic cholesterol and triglyceride metabolism by activating AMPK*α* to attenuate hypercholesterolemia

Jiaqi Li[a], Mingchao Wang[b], Kai Qu[b], Yuyao Sun[c,] Zequn Yin[a], Na Dong[a], Xin Sun[d], Yitong Xu[e], Liang Chen[f], Shuang Zhang[g], Xunde Xian[e], Suowen Xu[h i], Likun Ma[a], Yajun Duan[a,*], Haibo Zhu[b,*]

[a]*Department of Cardiology, the First Affiliated Hospital of USTC, Division of Life Sciences and Medicine, University of Science and Technology of China, Hefei 230001, China*

[b]*State Key Laboratory for Bioactive Substances and Functions of Natural Medicines, Beijing Key Laboratory of New Drug Mechanisms and Pharmacological Evaluation Study, Institute of Materia Medica, Chinese Academy of Medical Sciences and Peking Union Medical College, Beijing 100050, China*

[c]*College of Life Sciences, State Key Laboratory of Medicinal Chemical Biology, Key Laboratory of Bioactive Materials of Ministry of Education, Nankai University, Tianjin 300071, China*

[d]*State Key Laboratory of Common Mechanism Research for Major Diseases, Department of Biochemistry and Molecular Biology, Institute of Basic Medical Sciences, Chinese Academy of Medical Sciences and Peking Union Medical College, Beijing 100005, China*

[e]*Institute of Cardiovascular Sciences, State Key Laboratory of Vascular Homeostasis and Remodeling, School of Basic Medical Sciences, Peking University, Beijing 100083, China*

[f]*College of Life Science, Anhui Medical University, Hefei 230032, China*

[g]*Key Laboratory of Metabolism and Regulation for Major Diseases of Anhui Higher Education Institutes, College of Food and Biological Engineering, Hefei University of Technology, Hefei 230009, China*

[h]*Department of Endocrinology, the First Affiliated Hospital of USTC, Division of Life Sciences and Medicine, University of Science and Technology of China, Hefei 230001, China*

[i]*Anhui Provincial Key Laboratory of Metabolic Health and Panvascular Diseases, Hefei 23001, China*

Received 25 December 2024; received in revised form 26 January 2025; accepted 11 February 2025

*Corresponding authors.

E-mail addresses: zhuhaibo@imm.ac.cn (Haibo Zhu), yajunduan@ustc.edu.cn (Yajun Duan).

Running title: IMM-H007 reduces hypercholesterolemia and atherosclerosis

Abstract Hypercholesterolemia is a significant risk factor for the development of atherosclerosis. 2′,3′,5′-Tri-*O*-acetyl-N6-(3-hydroxyphenyl) adenosine (IMM-H007), a novel AMPK agonist, has shown protective effects in metabolic diseases. However, its impact on cholesterol and triglyceride metabolism in hypercholesterolemia remains unclear. In this study, we aimed to elucidate the effects and specific mechanisms by which IMM-H007 regulates cholesterol and triglyceride metabolism. To achieve this goal, we used *Apoe*$^{-/-}$ and *Ldlr*$^{-/-}$ mice to establish a hypercholesterolemia/atherosclerosis model. Additionally, hepatocyte-specific *Ampka*1/2 knockout mice were subjected to a 5-week high-cholesterol diet to establish hypercholesterolemia, while atherosclerosis was induced *via* AAV-*PCSK9* injection combined with a 16-

week high-cholesterol diet. Our results demonstrated that IMM-H007 improved cholesterol and triglyceride metabolism in mice with hypercholesterolemia. Mechanistically, IMM-H007 modulated the AMPKα1/2–LDLR signaling pathway, increasing cholesterol uptake in the liver. Furthermore, IMM-H007 activated the AMPKα1–FXR pathway, promoting the conversion of hepatic cholesterol to bile acids. Additionally, IMM-H007 prevented hepatic steatosis by activating the AMPKα1/2–ATGL pathway. In conclusion, our study suggests that IMM-H007 is a promising therapeutic agent for improving hypercholesterolemia and atherosclerosis through the activation of AMPKα.

KEY WORDS IMM-H007; AMPK; cholesterol; LDLR; FXR; Hypercholesterolemia; Triglyceride; Atherosclerosis

1. Introduction

Overconsumption of dietary fats and cholesterol leads to hypercholesterolemia, which pathologically elevates circulating low-density lipoprotein (LDL) cholesterol and triglyceride levels, consequently increasing atherosclerosis and cardiovascular disease risk[1-3]. Therefore, maintaining the homeostasis of cholesterol and triglycerides is crucial. The liver plays a central role in lipid metabolism. It can clear most of the excess LDL-cholesterol in the circulation through hepatic low-density lipoprotein receptor (LDLR) activity. Posttranslationally, the proprotein convertase subtilisin/kexin type 9 (PCSK9) and inducible degrader of LDLR (IDOL) promote the degradation of LDLR. Consequently, PCSK9 and IDOL represent promising targets for enhancing cholesterol metabolism[4-6]. Currently, several PCSK9 inhibitors are approved for treating primary hypercholesterolemia; however, effective IDOL inhibitors have yet to be discovered[7,8].

The liver eliminates cholesterol from the bloodstream by secreting bile[9]. Therefore, promoting the conversion of cholesterol into bile acids is a key strategy for regulating cholesterol metabolism. The farnesoid X receptor (FXR, NR1H4), a member of the nuclear receptor superfamily, is involved in regulating bile acid metabolism in the liver. FXR binds to the promoter of the nuclear receptor subfamily 0 group B member 2 (SHP, NR0B2) gene and regulates bile acid synthesis by inhibiting the rate-limiting enzyme cytochrome P450 family 7 subfamily A member 1 (CYP7A1) in the classical bile acid synthesis pathway and the metabolic enzyme cytochrome P450 family 27 subfamily A member 1 (CYP27A1) in the alternative pathway[10,11].

AMP-activated protein kinase (AMPK) is a serine/threonine protein kinase composed of α, β, and γ subunits that form a heterotrimeric complex. AMPK activation enhances triglyceride hydrolysis, promotes fatty acid oxidation, and inhibits fatty acid synthesis, processes closely linked to metabolic diseases[12]. However, the role of AMPK in cholesterol metabolism remains unclear. Some studies suggest that AMPK activation inhibits the transcription factor sterol regulatory element binding transcription factor 2 (SREBP2), thereby reducing the transcription of LDLR[12]. In contrast, other studies have indicated that AMPK activation increases LDLR expression, whereas its inhibition suppresses LDLR expression[13-17]. Given these conflicting findings, further investigation is needed to clarify the impact of AMPK activation on LDLR regulation. Additionally, studies have shown that AMPK activation can inhibit FXR transcriptional activity both *in vitro*

and *in vivo*, worsening liver damage in intrahepatic cholestasis models[18]. These results indicate that AMPK activation under hypercholesterolemic conditions may promote bile acid production through the suppression of FXR activity, consequently attenuating hepatic cholesterol accumulation. In conclusion, AMPK plays a vital role in cholesterol metabolism, and the use of AMPK agonists may represent a promising therapeutic strategy for treating lipid metabolism disorders.

2′,3′,5′-Tri-*O*-acetyl-N^6-(3-hydroxyphenyl) adenosine (IMM-H007) is a novel AMPK agonist[19]. *In vivo*, IMM-H007 is metabolized to H007-M1 and enters cells *via* a nucleoside transporter. Research indicates that after metabolism, IMM-H007 is primarily distributed to tissues such as the serum, heart, and liver[20]. As an AMPK agonist, IMM-H007 has several pharmacological effects through AMPK activation, including the suppression of inflammation, improvement of cardiac function, and amelioration of liver steatosis[21-24]. Additionally, studies suggest that IMM-H007 may improve atherosclerosis[25,26]. However, the effects and specific regulatory mechanisms of IMM-H007 on cholesterol and triglyceride metabolism in hypercholesterolemia remain unclear. In this study, we investigated the impact of IMM-H007 on cholesterol and triglyceride metabolism, focusing on the role of hepatic AMPKα in mediating the efficacy of IMM-H007.

2. Materials and methods

2.1. Reagents

IMM-H007 and its main metabolite, H007-M1, were kindly provided by Dr. Haibo Zhu (Institute of Material Medica, Chinese Academy of Medical Sciences and Peking Union Medical College). Rabbit anti-AMPKα1 (NB110-55457) monoclonal antibody was purchased from Novus Biologicals (Littleton, CO, USA). Rabbit anti-LDLR (Cat# 10785-1-AP), PCSK9 (Cat# 55206-1-AP), ABCG1 (Cat# 13578-1-AP), AMPKα2 (Cat# 18167-1-AP), AMPKβ (Cat# 10308-1-AP), AMPKγ (Cat# 10290-1-AP), FXR (Cat# 25055-1-AP), CREB1 (Cat# 12208-1-AP) polyclonal antibodies, mouse anti-FOXO1 (Cat# 66457-1), and HRP-conjugated GAPDH monoclonal antibodies (Cat# HRP-60004) were purchased from Proteintech Group Inc. (Chicago, IL, USA). Rabbit anti-DGAT1 (Cat# A6857), IDOL (Cat# A6166), SENP1 (Cat# A13086), β-actin (Cat# AC026), ABCA1 (Cat# A16337), AMPKα1/2 (Cat# A17290), CYP7A1 (Cat# A10615), and SHP (Cat#A16454) polyclonal antibodies were purchased from ABclonal Technology (Wuhan, Hubei, China). Rabbit anti-ATGL (Cat# SC-67355) polyclonal antibody and mouse anti-ABCB11 (Cat# SC-74500) were purchased from Santa Cruz Biotechnology (Dallas, TX, USA).

TRIzol reagent was purchased from Invitrogen (Carlsbad, CA, USA). The reverse transcription kit was purchased from Promega (Madison, WI). SYBR Green Master Mix was purchased from Bio-Rad (Los Angeles, CA, USA). FITC-conjugated goat anti-rabbit IgG (Cat# sc-2054) was purchased from Santa Cruz. FITC-conjugated goat anti-mouse IgG (Cat# F0257) was purchased from Sigma−Aldrich (St. Louis, MO, USA). All other reagents were purchased from Sigma–Aldrich.

2.2. Animals and study design

All animal care and experimental protocols were approved by the Ethics Committee of Nankai University and conformed to the Guide for the Care and Use of Laboratory Animals published by the NIH (Ethical approval number: 2023-SYDWLL-000614). Eight-week-old male apolipoprotein E-deficient (*Apoe*$^{-/-}$) mice were obtained from GemPharmatech (Jiangsu, China) and randomly divided into two groups (15 mice/group): HFHC groups, in which the mice were fed a high-fat and high-cholesterol (HFHC) diet containing 21% fat plus 0.5% cholesterol for 16 weeks; and a HFHC-H007 group, in which the mice were fed a HFHC for 10 weeks and then treated with IMM-H007 (200 mg/kg body weight/day) in combination with a HFHC for 6 weeks. The body weights of the mice were recorded from the 9th to the 16th weeks, and the food intake of the mice was measured at the 16th week. At the end of the experiment, the mice were euthanized, and the tissues were collected.

Eight-week-old male *Ldlr*$^{-/-}$ mice were obtained from GemPharmatech (Jiangsu, China) and randomly divided into two groups (8 mice/group). In the HFC group, the mice were fed an HFC (20% fat plus 1.25% cholesterol) for 20 weeks. In the IMM-H007 group, the mice were fed an HFC containing IMM-H007 (200 mg/kg body weight/day). The body weights of the mice were measured at the 20th week. At the end of the experiment, the mice were euthanized, and the tissues were collected.

Ampka$^{flox/flox}$ and hepatocyte *Ampka*1/2-deficient (h*Ampka* KO) mice aged 8–10 weeks were purchased from ViewSolid Biotech Company (Beijing, China) and randomly divided into four groups (5 mice/group): *Ampka*$^{flox/flox}$ mice were fed a high-fat (HF)/high-cholesterol (HC)/bile-salt (BS) diet (rodent diet with 40 kcal% fat, 1.25% cholesterol, 0.5% cholic acid; D12109C; Research Diets, New Brunswick, NJ, USA) with or without IMM-H007 (200 mg/kg body weight/day) for 5 weeks. h*Ampka* KO mice were fed a HF/HC/BS diet with or without IMM-H007 (200 mg/kg body weight/day) for 5 weeks.

Ampka$^{flox/flox}$ and hepatocyte *Ampka*1/2-deficient (h*Ampka* KO) mice aged 8–10 weeks were randomly divided into four groups (8 mice/group): *Ampka*$^{flox/flox}$ mice received AAV-*PCSK*9 *via* tail vein injection (2×10^{11} vg per mouse; WZ Biosciences Inc., Jinan, China) and then were fed a HF/HC/BS diet with or without IMM-H007 (200 mg/kg body weight/day) for 16 weeks. h*Ampka*-KO mice received AAV-*PCSK9* *via* tail vein injection and were then fed a HF/HC/BS diet with or without IMM-H007 (200 mg/kg body weight/day) for 16 weeks.

2.3. Cell culture

HepG2 cells were cultured in complete DMEM medium supplemented with 10% FBS, 50 μg/mL penicillin/streptomycin, and 2 mmol/L glutamine. HepG2 cells lacking *Ampka* expression were established *via* CRISPR (clustered regulatory interspaced short palindromic repeat)/CRISPR-Cas9 (associated protein 9) technology as described previously[27]. HepG2 cells lacking *Ampka* expression were defined as Cas9-*AMPKA* cells, and the corresponding control cells were defined as Cas9-Ctrl cells. Human aortic smooth muscle cells (HASMCs) were purchased from ATCC (Manassas, VA, USA) and cultured in DMEM/F12 (1:1) medium containing 10% FBS, 50 μg/mL penicillin/streptomycin, and 2 mmol/L glutamine. All the cells (~90% confluence) were treated with the corresponding serum-free medium.

2.4. Determination of hepatic lipid content

To determine the liver lipid content, a part of the liver was fixed, dehydrated, and processed according to standard protocols to prepare 5 μm frozen sections, followed by Oil Red O staining. Another piece of liver (~100 mg) was used to extract total lipids to determine the triglyceride or cholesterol content *via* the corresponding assay kits (Wako, Osaka, Japan) and was normalized to the protein content[28].

2.5. Determination of atherosclerotic lesions

All the aorta samples were collected from the mice after euthanasia as previously described, and the external connective tissue and fat were removed, followed by the determination of atherosclerotic lesions *via* Oil Red O staining[27]. Images of the aortas were obtained with a Leica M165FC stereoscopic microscope (Leica, Wetzlar, Germany), and the lesion areas were quantified *via* a computer-assisted image analysis method (Photoshop CS3) and are presented as percentages.

Aortic root frozen sections were prepared for Oli Red O staining to determine the extent of sinus lesions in the aortic root. After being photographed with a Leica DM5000B microscope (Leica, Wetzlar, Germany), the lesion areas were quantified *via* Photoshop CS3 and expressed as μm^2.

2.6. H&E, VVG, and immunofluorescence staining

To determine and quantify the area of the necrotic cores, the thickness of the fibrosis cap and the collagen content in the lesion areas, hematoxylin and eosin (H&E), Verhoeff-Van Gieson (VVG), and Masson staining were performed on frozen aortic root cross-sections[27]. After staining, the sections were mounted with resinous mounting medium. Images were taken with a Leica microscope. On the basis of the image of Masson staining, the necrotic core area, fibrous cap thickness of the lesions, or collagen-positive area were quantified with Photoshop CS3 and are expressed as percentages.

2.7. Western blot and quantitative real-time PCR (qRT-PCR)

Total, cytoplasm, and nuclear proteins were extracted from liver tissue or cells, after which Western blotting was performed to determine the expression of the indicated proteins. The target bands were normalized to those of GAPDH or *β*-actin in the corresponding samples.

Total RNA was extracted from tissues or cells, followed by reverse transcription to cDNA *via* RT SuperMix. The expression of mRNA was determined by qRT-PCR *via* SYBR Green Master Mix with the primers listed in Supporting Information Table S1 and normalized to the expression of *GAPDH* mRNA in the corresponding samples.

2.8. Inhibition of gene expression by siRNA

siRNAs against human *IDOL* (*MYLIP*) (siG150715053038-1-5) and *SENP1* (siB131111164859-1-5) were purchased from RIBOBIO (Guangzhou, China). siRNAs against human *AMPKA1*, *AMPKA2*, *AMPKB* and *AMPKG* were purchased from Tsingke Biotechnology (Beijing, China). HepG2 cells were transfected with siRNA *via* Lipofectamine RNAiMAX Transfection Reagent (Invitrogen, Grand Island, NE, USA). After 48

h of transfection, the cells were switched to complete DMEM without sodium pyruvate for another 24 h and then treated with H007-M1 at the indicated concentration in serum-free medium for 24 h, followed by determination of protein expression *via* Western blotting [29].

2.9. Determination of serum biochemical parameters

To collect the serum, blood samples were collected and stored at room temperature for 2 h and centrifuged at 2000 × *g* at room temperature for 20 min. Serum was collected and used to determine the levels of triglycerides, total cholesterol, and HDL-cholesterol with an automatic biochemical analyzer (Model 7020; Hitachi, Tokyo, Japan). The non-HDL can be calculated according to Eq. (1):

non-HDL cholesterol (non-HDL) = Total cholesterol−HDL cholesterol (1)

2.10. Metabolic studies

After 15 weeks of treatment, O_2 consumption and CO_2 production were assessed during a 24-h light plus dark cycle *via* an open-flow respirometry system (TSE LabMaster, TSE Systems, Bad Homburg, Germany)[30]. Briefly, each animal was placed in a transparent plastic chamber (19.5 cm×9.2 cm×14.0 cm) with small pieces of tissue paper just enough to absorb animal waste. An incubator (MIR-553, SANYO, Japan) was used to maintain the chamber at a constant ambient temperature. Air from outside the building was pumped through the chamber at a mass flow rate of 0.81 min^{-1}. The energy expenditure (EE) value was calculated according to Eqs. (2) and (3):

$$RER=V_{CO2}/V_{O2} \quad (2)$$

$$EE= (3.815+1.232\times RER) \times V_{O2} \quad (3)$$

2.11. Statistical analysis

All experiments were repeated at least three times, and representative results are presented. The data are presented as the mean ± standard error of mean (SEM) and were analyzed by Student's *t* test or ANOVA with a *post hoc* test *via* GraphPad Prism software (San Diego, CA, USA). The differences were considered significant at $P < 0.05$.

3. Results

3.1. IMM-H007 inhibits hypercholesterolemia and atherosclerosis in apolipoprotein E-deficient (Apoe$^{-/-}$) mice

To investigate the role of IMM-H007 in lipid metabolism, eight-week-old male *Apoe*$^{-/-}$ mice were subjected to a 10-week high-fat, high-cholesterol (HFHC) diet to induce hypercholesterolemia. One group subsequently received IMM-H007 supplementation for 6 weeks while the HFHC diet was maintained (Fig. 1A). Compared to the HFHC group, mice treated with IMM-H007 (200 mg/kg body weight/day, HFHC-H007 group) showed reduced weight gain (Fig. 1B). IMM-H007 treatment had a minimal effect on food intake (Supporting Information Fig. S1A). Additionally, IMM-H007 treatment increased the energy consumption rate of the mice (Fig. S1B and S1C). Serum total cholesterol (TC) and non-high-density

lipoprotein (HDL) cholesterol levels were significantly lower in the HFHC-H007 group than in the HFHC group (Fig. 1C and D). However, there was no significant effect on HDL-cholesterol levels in the HFHC-H007 group (Fig. 1E). The serum triglyceride level was also lower in the HFHC-H007 group than in the HFHC group (Fig. 1F).

Dysregulation of cholesterol metabolism is known to contribute to atherosclerosis. The plaque area was significantly reduced in the HFHC-H007 group (Fig. 1G and H). Similarly, sinus lesions in the aortic root were decreased in the HFHC-H007 group (Fig. 1I and J). These results indicate that IMM-H007 can inhibit plaque development. Hematoxylin and eosin (HE) staining and Masson staining revealed a reduction in the necrotic core area and an increase in the fibrous cap area of plaques in the HFHC-H007 group (Fig. 1K–N). Masson staining and Verhoeff–van Gieson (VVG) staining revealed that IMM-H007 significantly increased the collagen content within plaques (Figure 1L, O, and P). Overall, these findings suggest that IMM-H007 effectively increases cholesterol levels, inhibits triglyceride accumulation, and reduces atherosclerotic plaques in *Apoe*$^{-/-}$ mice.

Insert Fig. 1

3.2. Ldlr deficiency prevented the hypercholesterolemia improvements induced by IMM-H007

The *Ldlr* knockout mouse is another widely utilized model for studying hypercholesterolemia and atherosclerosis[31]. To establish this disease model, we fed *Ldlr*-deficient mice a high-fat, high-cholesterol (HFC) diet (containing 20% fat and 1.5% cholesterol) to induce hypercholesterolemia and atherosclerosis (Fig. 2A). IMM-H007 did not significantly affect body weight at the end of the experiment (Fig. 2B). In contrast to the findings in *Apoe*$^{-/-}$ mice, IMM-H007 did not significantly affect TC ($P = 0.054$), non-HDL-cholesterol ($P = 0.075$), or HDL-cholesterol ($P = 0.26$) in *Ldlr*$^{-/-}$ mice (Fig. 2C–E), suggesting that IMM-H007 may improve cholesterol levels through LDLR. Moreover, IMM-H007 significantly reduced triglyceride levels in *Ldlr*$^{-/-}$ mice (Fig. 2F). Compared with HFC diet feeding, IMM-H007 treatment inhibited *en face* aortic lesions (Fig. 2G). The area of sinus lesions also decreased in the HFC-H007 group (Fig. 2H and I). Additionally, HE staining and Masson's trichrome staining revealed that IMM-H007 significantly reduced the necrotic core area and increased the fibrous cap area in plaques (Fig. 2J–M). Masson staining further revealed that IMM-H007 significantly increased the collagen content within the plaques (Fig. 2K and N). In conclusion, these findings suggest that while the regulation of cholesterol by IMM-H007 appears to be LDLR dependent, additional LDLR-independent mechanisms may contribute to plaque improvement.

Insert Fig. 2

3.3. IMM-H007 regulates LDLR by activating AMPKα

LDL cholesterol and very low-density lipoprotein (VLDL) cholesterol are the primary components of non-HDL cholesterol. LDLR, a receptor located on hepatocyte surfaces, plays a crucial role in clearing LDL and VLDL particles from the circulation[32]. We found that IMM-H007 increased LDLR protein expression in the livers of *Apoe*$^{-/-}$ mice (Fig. 3A). Pharmacological studies have shown that IMM-H007 undergoes gradual

deacetylation in plasma, with the primary metabolite being H007-M1, which has lost three acetyl groups[33,34]. We treated HepG2 cells with H007-M1 and found that H007-M1 promoted LDLR expression *in vitro* (Fig. 3B). We subsequently treated HepG2 cells with H007-M1 and AICAR (5-aminoimidazole-4-carboxamide 1-β-D-ribofuranoside), both pharmacological activators of AMPK, in combination with cycloheximide (CHX), a protein synthesis inhibitor. CHX accelerated LDLR degradation, whereas both H007-M1 and AICAR increased LDLR stability (Fig. 3C and Supporting Information Fig. S2). Next, we inhibited various AMPK subunits to determine their role in this process. Our results revealed that the inhibition of AMPKα1 and AMPKα2 blocked IMM-H007-induced LDLR expression, whereas the inhibition of AMPKγ and AMPKβ did not affect LDLR levels (Fig. 3D–K). In summary, these findings suggest that IMM-H007 increases LDLR stability through the activation of AMPKα1/2.

Insert Fig. 3

3.4. Hepatocyte-specific Ampka1/2 knockout inhibits the ameliorative effects of IMM-H007 on hypercholesterolemia

To further validate the role of hepatic AMPKα in IMM-H007-mediated lipid metabolism, we generated hepatocyte-specific *Ampka*1/2-deficient (h*Ampka* KO) mice (Supporting Information Fig. S3) and subjected *Ampka*$^{flox/flox}$ mice and h*Ampka* KO mice to a high-fat, high-cholesterol diet for five weeks (Fig. 4A). The results revealed that IMM-H007 significantly decreased TC and non-HDL cholesterol levels but had no significant effect on HDL cholesterol levels in *Ampka*$^{flox/flox}$ mice (Fig. 4B–D). Additionally, IMM-H007 improved triglyceride levels (Fig. 4E). However, in h*Ampka* KO mice, the regulatory effects of IMM-H007 on cholesterol and triglycerides were abolished (Fig. 4B–E). Furthermore, we performed transcriptome sequencing on the livers of the mice. The results revealed that in *Ampka*$^{flox/flox}$ mice, IMM-H007 significantly regulated the cholesterol and glycerolipid metabolism pathways. However, these pathways did not significantly change in h*Ampka* KO mice (Fig. 4F). Moreover, IMM-H007 upregulated LDLR expression in the livers of *Ampka*$^{flox/flox}$ mice but did not affect LDLR expression in h*Ampka* KO mice (Fig. 4G and H). These results demonstrate that IMM-H007 increases LDLR expression in the liver through AMPKα1/2-dependent mechanisms.

Insert Fig. 4

3.5. IMM-H007 increases LDLR expression via the AMPKα1/2-small ubiquitin-like modifier-specific protease 1 (SENP1)–IDOL pathway

Mechanistic studies have established that both PCSK9 and IDOL posttranslationally promote LDLR degradation through distinct ubiquitination pathways[35,36]. In HepG2 cells, we determined that siRNA targeting *IDOL*, but not *PCSK9*, abolished the H007-M1-induced increase in LDLR expression (Fig. 5A and B). Furthermore, H007-M1 did not affect the transcription of *PCSK9* or *IDOL* in HepG2 cells (Fig. 5C). These results suggest that IMM-H007 regulates LDLR through IDOL rather than PCSK9 at the posttranscriptional level.

SUMOylation of IDOL at the K293 residue inhibits its autoubiquitination and increases its protein level. Conversely, SENP1 deSUMOylates IDOL, leading to a decrease in its protein level[37]. We found that H007-M1 inhibits IDOL SUMOylation. (Fig. 5D). Moreover, inhibiting *SENP1* expression abolished the effect of H007-M1 on IDOL and LDLR levels in HepG2 cells (Fig. 5E). Thus, IMM-H007 induces LDLR expression *via* the SENP1–IDOL signaling pathway.

Recent studies have reported that AMPK activates SENP1 in T cells and proximal tubular epithelial cells (PTECs)[38,39]. We observed that H007-M1 decreased IDOL expression and increased SENP1 expression in control HepG2 cells (Cas9-*Ctrl*) but not in *AMPKA*-deficient HepG2 cells (Cas9-*AMPKA*) (Fig. 5F). Additionally, IMM-H007 increased SENP1 protein expression and decreased IDOL expression in the liver, whereas hepatocyte-specific *Ampka*1/2 deficiency abolished these changes, indicating that IMM-H007 regulates SENP1–IDOL through AMPK*α* activation (Fig. 5G). Moreover, H007-M1 promoted *SENP1* transcription in an AMPK*α*1/2-dependent manner (Fig. 5H). Consistently, the overexpression of *AMPKA*1/2 promoted the transcription of *SENP1* (Supporting Information Fig. S4A). To further elucidate the mechanism, we used multiple databases, including Jaspar, GeneCards, CritromeDB, and hTFtarget, to predict potential transcription factors that may regulate *SENP1* transcription. Through this analysis, we identified two transcription factors, with cyclic AMP response element-binding protein 1 (CREB1) being the only one activated by AMPK (Fig. S4B). CREB1 has already been shown to be phosphorylated by AMPK and to promote the transcription of downstream genes[40]. Our experiments confirmed that H007-M1 treatment promoted the nuclear expression of CREB1 in HepG2 cells (Fig. S4C). We also predicted *via* the JASPAR database that the *SENP1* promoter contains binding sites for CREB1. ChIP assays further confirmed that both H007-M1 treatment and *AMPKA*1/2 overexpression increased CREB1 binding to the *SENP1* promoter (Fig. S4D). To refine the identification of the binding site, we constructed plasmids with mutated binding sites and performed luciferase assays. The results demonstrated that both H007-M1 treatment and *AMPKA*1/2 overexpression could activate the *SENP1* promoter, but this activation was abolished when the predicted binding site was mutated (Fig. 5I and J). Thus, IMM-H007, through AMPK*α* activation, enhances CREB1 activity, leading to an increase in *SENP1* transcription.

Finally, we used *Apoe*$^{-/-}$ mice with atherosclerosis to confirm that the AMPK*α*–SENP1–IDOL–LDLR signaling pathway is activated in the liver by IMM-H007 (Supporting Information Fig. S5). Taken together, these findings indicate that IMM-H007 enhances LDLR stability through activation of the AMPK*α*–CREB1–SENP1–IDOL pathway (Fig. S4E).

Insert Fig. 5

3.6. IMM-H007 increases hepatic cholesterol metabolism via the AMPKα1–FXR–SHP–CYP7A1/CYP27A1 pathway

The conversion of cholesterol into bile acids is the major mechanism for its elimination from the body[41]. To further delineate the effects of IMM-H007 on postuptake hepatic cholesterol metabolism, we analyzed the transcriptional regulation of bile acid metabolic pathways. As depicted in Fig. 6A, compared with those in the *Ampka*$^{flox/flox}$ group, *Cyp7a1* and *Cyp27a1* levels were significantly increased in *Ampka*$^{flox/flox}$-H007 mice,

whereas *Fxr*, *Shp*, ATP-binding cassette subfamily B member (*Abcb*)11, and *Abcb4* levels were significantly decreased. However, IMM-H007 did not significantly affect the expression of these genes in h*Ampka* KO mice (Fig. 6A). We also assessed the protein levels of these genes in the liver. Consistent with the results of the transcriptional analysis, the CYP7A1 and CYP27A1 levels were significantly higher in *Ampka*$^{flox/flox}$-H007 mice than in *Ampka*$^{flox/flox}$ mice, whereas the FXR and SHP levels were significantly lower. IMM-H007 had no significant effect on the expression of these proteins in h*Ampka* KO mice. Additionally, IMM-H007 did not significantly alter the expression of ABCB11 or ABCB4, indicating that other posttranslational regulatory mechanisms might be involved (Fig. 6B). Moreover, H007-M1 significantly inhibited the activity of the *FXR* promoter, suggesting that H007-M1 can regulate *FXR* transcription (Fig. 6C).

Further investigations involved the inhibition of different AMPKα subunits. The results demonstrated that inhibiting *Ampka*1 blocked the induction of CYP7A1, CYP27A1, FXR, and SHP by H007-M1, whereas inhibiting *Ampka*2 did not affect protein expression (Fig. 6D–G). Furthermore, liver cholesterol levels were significantly lower in *Ampka*$^{flox/flox}$-H007 mice than in *Ampka*$^{flox/flox}$ mice, accompanied by an increase in bile acid levels (Fig. 6H and I). This finding suggests an increased conversion of cholesterol to bile acids in the liver. In contrast, H007-M1 had no significant effect on liver cholesterol or bile acid levels in h*Ampka* KO mice (Fig. 6H and I). In summary, IMM-H007 promotes hepatic cholesterol metabolism through the activation of the AMPKα1–FXR–SHP–CYP7A1/CYP27A1 pathway (Supporting Information Fig. S6).

Insert Fig. 6

3.7. IMM-H007 promotes liver triglyceride hydrolysis by activating AMPKα1/2

IMM-H007 regulated glycerolipid metabolism in *Ampka*$^{flox/flox}$ mice but not in hepatocyte-specific *Ampka*1/2 KO mice, indicating AMPKα-dependent hepatic lipid modulation (Fig. 4F). In *Ampka*$^{flox/flox}$ mice, IMM-H007 significantly improved the pale coloration of the liver. In contrast, IMM-H007 did not improve liver color in h*Ampka* KO mice (Fig. 7A). HE and Oil Red O staining demonstrated that IMM-H007 significantly reduced hepatic lipid deposition in *Ampka*$^{flox/flox}$ mice, whereas this inhibitory effect was abolished in h*Ampka* KO mice (Fig. 7B and C). Additionally, IMM-H007 reduced liver triglyceride levels in *Ampka*$^{flox/flox}$ mice. However, hepatocyte-specific *Ampka* deficiency prevented the decrease in triglyceride levels induced by IMM-H007 (Fig. 7D). Liver pallor and excessive lipid accumulation in both *Apoe*$^{-/-}$ and *Ldlr*$^{-/-}$ mice were also improved by IMM-H007 (Supporting Information Figs. S7A–S7D and S8A–S8D).

Mechanistically, IMM-H007 increased both the protein and mRNA expression of adipose triglyceride lipase (ATGL), a key enzyme that promotes the breakdown of triglycerides into fatty acids. Hepatocyte-specific *Ampka*1/2 deficiency abolished IMM-H007-induced ATGL upregulation (Fig. 7E and F). Additionally, IMM-H007 did not significantly affect the expression of acyl-CoA: diacylglycerol acyltransferase 1 (DGAT1), the key enzyme involved in triglyceride synthesis (Fig. 7F). We also found that IMM-H007 upregulated ATGL expression but did not affect DGAT1 levels in the livers of *Apoe*$^{-/-}$ and *Ldlr*$^{-/-}$ mice (Figs. S7E, S7F and S8E, S8F). Moreover, H007-M1 increased ATGL expression in Cas9-*Ctrl* cells, whereas *AMPKA* deficiency abolished H007-M1-induced ATGL upregulation (Fig. 7G). AMPK activation promotes triglyceride hydrolysis possibly through regulating forkhead box protein O1 (FOXO1)[42,43]. We

observed that IMM-H007 modulated FOXO1 activity (Supporting Information Fig. S9), suggesting FOXO1 may contribute to the improvement of triglyceride metabolism. In summary, these results suggest that IMM-H007 affects liver lipid accumulation through the AMPKα1/2–ATGL pathway (Fig. 7H).

Insert Fig. 7

3.8. Hepatocyte-specific Ampka1/2 deficiency prevented the improvements in atherosclerosis induced by IMM-H007

To further investigate the role of hepatic AMPKα in the treatment of atherosclerosis with IMM-H007, we induced atherosclerosis in h*Ampka* KO mice by injecting adeno-associated virus (AAV)-*PCSK9* and feeding them an atherogenic diet for 16 weeks (Fig. 8A)[44]. As anticipated, AAV-*PCSK9* injection increased human PCSK9 expression in the serum (Supporting Information Fig. S10). IMM-H007 modestly reduced TC and non-HDL cholesterol while significantly lowering triglyceride levels in the serum (Fig. 8B–E). Compared with the *Ampka*$^{flox/flox}$ group, IMM-H007 significantly reduced the number of *en face* aortic lesions in the *Ampka*$^{flox/flox}$-H007 group. However, hepatocyte-specific *Ampka*1/2 deficiency abolished the decrease in the lesion area (Fig. 8F). Similarly, IMM-H007 reduced the number of sinus lesions, but this effect was abolished by hepatocyte-specific *Ampka*1/2 deficiency (Fig. 8G and H). Interestingly, HE and Masson staining revealed that hepatocyte-specific *Ampka*1/2 deficiency did not affect the impact of IMM-H007 on the necrotic core or fibrous cap area or the collagen content (Fig. 8I–M). In summary, the inhibition of the atherosclerotic plaque area by IMM-H007 relies primarily on hepatic *Ampka*1/2 expression. Nonetheless, IMM-H007 also appears to act *via* mechanisms independent of AMPK to regulate plaque stability.

Insert Fig. 8

3.9. IMM-H007 inhibits macrophage and smooth muscle cell foaming by activating ABCA1/ABCG1

Notably, even in *Ampka*1/2 deficient mice, IMM-H007 still reduced the area of the plaque necrotic core and increased the fibrous cap and collagen-positive areas (Fig. 8I–M). The main components of the necrotic core are foam cells derived from macrophages and smooth muscle cells (SMCs) that engulf lipids[45]. Additionally, SMCs play crucial roles in forming fibrous caps and secreting collagen[46]. To investigate this further, we treated macrophages and human aortic smooth muscle cells (HASMCs) with H007-M1 and oxidized low-density lipoprotein (oxLDL), followed by Oil Red O staining. Loading oxLDL into macrophages and HASMCs significantly increased the number of Oil Red O-positive cells. Moreover, H007-M1 reduced foam cell formation in both macrophages and HASMCs (Supporting Information Figs. S11A and S12A). At the molecular level, ATP-binding cassette transporter A1 (ABCA1) and ABCG1 are crucial for mediating cholesterol efflux and reducing foam cell formation. We observed that H007-M1 upregulated the protein expression of ABCA1 and ABCG1 both in the presence and absence of oxLDL (Fig. S11B, S11C and S12B, S12C). Additionally, H007-M1 also increased the mRNA levels of *ABCA1* and *ABCG1*, regardless of the presence of oxLDL (Figs. S11D, S11E and S12D, S12E). In summary, these results indicate that H007-M1 reduces the formation of foam cells derived from macrophages and smooth muscle cells, primarily by increasing ABCA1/G1 expression and promoting cholesterol efflux.

4. Discussion

While various AMPK agonists have demonstrated efficacy in treating atherosclerosis, each is associated with certain limitations. For example, metformin is frequently associated with gastrointestinal side effects[47] and has shown limited efficacy in patients with nonalcoholic fatty liver disease[48]. Cordycepin, another AMPK activator, is rapidly deaminated by adenosine deaminase *in vivo*, resulting in a shortened half-life and reduced bioavailability[49]. Additionally, cordycepin can cause side effects such as headaches, diarrhea, and allergic reactions[50]. Therefore, there is a need to develop new and more effective AMPK activators for treating metabolic diseases. IMM-H007, a compound derived from cordycepin, activates AMPK with low toxicity. Previous research has demonstrated that IMM-H007 outperforms both metformin and AICAR in treating atherosclerosis[51]. These findings underscore the need for further investigation into the therapeutic effects and mechanisms of IMM-H007 in treating hypercholesterolemia.

IMM-H007 contains three acetyl groups, which are prone to rapid hydrolysis by plasma esterase[33]. High-performance liquid chromatography analysis identified five potential hydrolysis products of IMM-H007 (M1–M5) in rodent and mammalian plasma. Among these, N^6-(3-hydroxylaniline) adenosine (H007-M1, M1) has emerged as the active form of IMM-H007 *in vivo*[34]. A study demonstrated that the liver is a primary distribution site for IMM-H007 following its metabolism *in vivo*[20]. Peng et al.[23] demonstrated that IMM-H007 can activate AMPK and its downstream molecules in hepatocytes after metabolism. Additionally, in *Apoe*-knockout mice, IMM-H007 activated AMPK expression in the liver[19]. Molecular docking experiments further confirmed that IMM-H007 binds directly to AMPK after metabolism, promoting its activation. H007-M1 forms hydrogen bonds with hr86, Thr88, Asp89, Lys126, Lys148, and His150 in AMP binding site-1 and Asp244, Arg268, Gly274, and Arg298 in AMP binding site-3[52]. In conclusion, the results of the present study indicate that, after metabolism, IMM-H007 can directly increase AMPK activity in the liver.

In this study, we demonstrated the role of IMM-H007 in liver cholesterol uptake. Specifically, we showed that IMM-H007 functions as an IDOL inhibitor, regulating LDLR expression and thereby promoting liver cholesterol uptake. Under normal chow conditions, $Idol^{-/-}$ mice exhibit minimal lipid metabolic changes[53]. These findings suggest that IDOL may play a complex role in cholesterol metabolism regulation, which warrants further investigation. We plan to conduct additional studies to provide *in vivo* evidence of the effects of IMM-H007 on IDOL and its role in the function of IMM-H007.

PCSK9 inhibitors (*e.g.*, alirocumab and evolocumab) are also known to effectively improve LDL-cholesterol levels[54,55]. PCSK9 binds to LDLR, leading to lysosomal degradation of the receptor, whereas IDOL reduces LDLR levels through polyubiquitination and subsequent lysosomal degradation[56]. Therefore, combining IMM-H007 with PCSK9 inhibitors may offer a complementary approach to lowering blood cholesterol. Moreover, PCSK9 inhibitors can increase alanine or aspartate transaminase levels up to 3× the upper limit of normal[57]. In contrast, IMM-H007 metabolites have been shown to improve liver function and reduce transaminase levels[21]. Thus, the combined use of IMM-H007 and PCSK9 inhibitors could mitigate the side effects associated with PCSK9 inhibitors.

Lipoproteins are macromolecular complexes composed of apolipoproteins and lipids that solubilize hydrophobic lipids in the bloodstream for systemic transport. Because of differences in lipoprotein distribution and structure between humans and mice, clinical assay kits designed for humans cannot directly measure mouse LDL-cholesterol. However, owing to limitations in sample size, we could not perform serum fast protein liquid chromatography analysis in *Apoe* and *Ldlr* knockout mice, but we plan to address this in future experiments. Moreover, in our lipoprotein analysis, we did not observe changes in HDL levels. However, Huang et al.[58] reported that six weeks of IMM-H007 treatment in Paigen diet-fed *Apoe*$^{-/-}$ mice increased the level of circulating HDL. Additionally, two weeks of IMM-H007 treatment in Paigen diet-fed wild-type mice also resulted in increased HDL levels. These discrepancies may be attributed to the longer modeling period and shorter duration of drug administration in our study, which might have led to a more severe model. Differences in the composition of the feed could also have influenced cholesterol levels.

In conclusion, our findings indicate that IMM-H007 activates AMPKα to modulate hepatic cholesterol uptake and metabolism and improve triglyceride metabolism, ultimately contributing to the alleviation of hypercholesterolemia and atherosclerosis.

5. Conclusions

The inhibition of hypercholesterolemia and atherosclerosis by IMM-H007 involves the following mechanisms: 1) regulating the AMPKα1/2–LDLR signaling pathway to improve cholesterol uptake; 2) promoting hepatic cholesterol efflux *via* the AMPKα1–FXR–CYP7A1/CYP27A1 pathway; and 3) regulating TG metabolism by activating the AMPKα1/2−ATGL pathway.

Acknowledgments

This work was supported by National Key Research and Development Program of China Grants 2021YFC2500506 to Yajun Duan, National Natural Science Foundation of China (NSFC) Grants U22A20272 and 82173807 to Yajun Duan, Chinese Academy of Medical Sciences Innovation Fund for Medical Sciences (No. 2021-I2M-1-028, China), National Natural Science Foundation of China Grants 82073837, the Fundamental Research Funds for the Central Universities WK9100000064 (China), and USTC Research Funds of the Double First-Class Initiative (YD9110002089, China). Unfortunately, one of our corresponding authors, Prof. Haibo Zhu, passed away *in* 2024. IMM-H007 and H007-M1 were kindly provided by Professor Haibo Zhu from Chinese Academy of Medical Sciences and Peking Union Medical College.

Author contributions

Haibo Zhu and Yajun Duan designed the study and edited the manuscript; Jiaqi Li and Yajun Duan drafted the manuscript; Jiaqi Li and Yuyao Sun collected the data and performed most of the experiments; Mingchao Wang and Kai Qu analyzed the data; Zequn Yin, Na Dong, Liang Chen, Yitong Xu, Xin Sun and Shuang Zhang assisted with the experimental operation. Haibo Zhu, Yajun Duan, Xunde Xian, Suowen Xu provided suggestions for the experimental procedure.

Conflicts of interest

The authors declare no conflicts of interest.

References

1 Defesche JC, Gidding SS, Harada-Shiba M, Hegele RA, Santos RD, Wierzbicki AS. Familial hypercholesterolaemia. *Nat Rev Dis Primers* 2017;**3**:17093.

2 Zhao H, Li Y, He L, Pu W, Yu W, Li Y, et al. *In vivo* AAV-CRISPR/Cas9-mediated gene editing ameliorates atherosclerosis in familial hypercholesterolemia. *Circulation* 2020;**141**:67-79.

3 Gofman JW, Lindgren F. The role of lipids and lipoproteins in atherosclerosis. *Science* 1950;**111**:166-71.

4 van Loon NM, Lindholm D, Zelcer N. The E3 ubiquitin ligase inducible degrader of the LDL receptor/myosin light chain interacting protein in health and disease. *Curr Opin Lipidol* 2019;**30**:192-7.

5 Melendez QM, Krishnaji ST, Wooten CJ, Lopez D. Hypercholesterolemia: the role of PCSK9. *Arch Biochem Biophys* 2017;**625-626**:39-53.

6 Chait A, Eckel RH. Lipids, lipoproteins, and cardiovascular disease: clinical pharmacology now and in the future. *J Clin Endocrinol Metab* 2016;**101**:804-14.

7 Petroglou D, Kanellos I, Savopoulos C, Kaiafa G, Chrysochoou A, Skantzis P, et al. The LDL-receptor and its molecular properties: from theory to novel biochemical and pharmacological approaches in reducing LDL-cholesterol. *Curr Med Chem* 2020;**27**:317-33.

8 Glueck CJ, Shah P, Goldenberg N, Prince M, Lee K, Jetty V, et al. Eligibility for PCSK9 treatment in 734 hypercholesterolemic patients referred to a regional cholesterol treatment center with LDL cholesterol ≥ 70 mg/dL despite maximal tolerated cholesterol lowering therapy. *Lipids Health Dis* 2016;**15**:55.

9 Henkel AS, Kavesh MH, Kriss MS, Dewey AM, Rinella ME, Green RM. Hepatic overexpression of abcb11 promotes hypercholesterolemia and obesity in mice. *Gastroenterology* 2011;**141**:1404-11, 11.e1-2.

10 Chiang JYL, Ferrell JM. Discovery of farnesoid X receptor and its role in bile acid metabolism. *Mol Cell Endocrinol* 2022;**548**:111618.

11 Cao Y, Xiao Y, Zhou K, Yan J, Wang P, Yan W, et al. FXR agonist GW4064 improves liver and intestinal pathology and alters bile acid metabolism in rats undergoing small intestinal resection. *Am J Physiol Gastrointest Liver Physiol* 2019;**317**:G108-15.

12 Herzig S, Shaw RJ. AMPK: guardian of metabolism and mitochondrial homeostasis. *Nat Rev Mol Cell Biol* 2018;**19**:121-35.

13 Sui GG, Xiao HB, Lu XY, Sun ZL. Naringin activates AMPK resulting in altered expression of SREBPs, PCSK9, and LDLR to reduce body weight in obese C57BL/6J mice. *J Agric Food Chem* 2018;**66**:8983-90.

14 Zhang F, Sun W, Chen J, Jiang L, Yang P, Huang Y, et al. SREBP-2, a new target of metformin?. *Drug Des Devel Ther* 2018;**12**:4163-70.

15 Liu S, Jing F, Yu C, Gao L, Qin Y, Zhao J. AICAR-induced activation of AMPK inhibits TSH/SREBP-2/HMGCR pathway in liver. *PLoS One* 2015;**10**:e0124951.

16 Li Z, Jiang JD, Kong WJ. Berberine up-regulates hepatic low-density lipoprotein receptor through Ras-

independent but AMP-activated protein kinase-dependent Raf-1 activation. *Biol Pharma Bull* 2014;**37**:1766-75.

17 Bian Y, Li X, Li X, Ju J, Liang H, Hu X, et al. Daming capsule, a hypolipidaemic drug, lowers blood lipids by activating the AMPK signalling pathway. *Biomed Pharmacother* 2019;**117**:109176.

18 Lien F, Berthier A, Bouchaert E, Gheeraert C, Alexandre J, Porez G, et al. Metformin interferes with bile acid homeostasis through AMPK–FXR crosstalk. *J Clin Invest* 2014;**124**:1037-51.

19 Ma A, Wang D, An Y, Fang W, Zhu H. Comparative transcriptomic analysis of mice liver treated with different AMPK activators in a mice model of atherosclerosis. *Oncotarget* 2017;**8**:16594-604.

20 Jin M, Guo N, Li T, Liu X, Sun S, Jin X, et al. Comprehensive characterization of *in vitro* and *in vivo* metabolites of 2′,3′,5′-tri-*O*-acetyl-N^6-(3-hydroxyphenyl) adenosine and study of the metabolites distribution in rats by combined methods of HPLC-DAD, off-line cryoNMR, and HPLC–QTOFMS. *J Chromatogr B Analyt Technol Biomed Life Sci* 2018;**1096**:187-200.

21 Li J, Chen B, Zhong L, Gao F, Zhu H, Wang F. AMP-activated protein kinase agonist N^6-(3-hydroxyphenyl)adenosine protects against fulminant hepatitis by suppressing inflammation and apoptosis. *Cell Death Dis* 2018;**9**:37.

22 Ge W, Zhang W, Gao R, Li B, Zhu H, Wang J. IMM-H007 improves heart function *via* reducing cardiac fibrosis. *Eur J Pharmacol* 2019;**857**:172442.

23 Peng X, Li J, Wang M, Qu K, Zhu H. A novel AMPK activator improves hepatic lipid metabolism and leukocyte trafficking in experimental hepatic steatosis. *J Pharmacol Sci* 2019;**140**:153-61.

24 Shi H, Wang Q, Yang L, Xie S, Zhu H. IMM-H007, a new therapeutic candidate for nonalcoholic fatty liver disease, improves hepatic steatosis in hamsters fed a high-fat diet. *FEBS Open Bio* 2017;**7**:1379-91.

25 Yu J, Ming H, Li HY, Yu B, Chu M, Zhu H, et al. IMM-H007, a novel small molecule inhibitor for atherosclerosis, represses endothelium inflammation by regulating the activity of NF-*κ*B and JNK/AP1 signaling. *Toxicol Appl Pharmacol* 2019;**381**:114732.

26 Wang MJ, Peng XY, Lian ZQ, Zhu HB. The cordycepin derivative IMM-H007 improves endothelial dysfunction by suppressing vascular inflammation and promoting AMPK-dependent eNOS activation in high-fat diet-fed ApoE knockout mice. *Eur J Pharmacol* 2019;**852**:167-78.

27 Ma C, Zhang W, Yang X, Liu Y, Liu L, Feng K, et al. Functional interplay between liver X receptor and AMP-activated protein kinase α inhibits atherosclerosis in apolipoprotein E-deficient mice—a new anti-atherogenic strategy. *Br J Pharmacol* 2018;**175**:1486-503.

28 Zhao D, Li J, Xue C, Feng K, Liu L, Zeng P, et al. TL1A inhibits atherosclerosis in apoE-deficient mice by regulating the phenotype of vascular smooth muscle cells. *J Biol Chem* 2020;**295**:16314-27.

29 Liu L, Zeng P, Yang X, Duan Y, Zhang W, Ma C, et al. Inhibition of vascular calcification. *Arterioscler Thromb Vasc Biol* 2018;**38**:2382-95.

30 Yang DB, Li L, Wang LP, Chi QS, Hambly C, Wang DH, et al. Limits to sustained energy intake. XIX. A test of the heat dissipation limitation hypothesis in Mongolian gerbils (*Meriones unguiculatus*). *J Exp Biol* 2013;**216**:3358-68.

31 Yang Y, Feng K, Yuan L, Liu Y, Zhang M, Guo K, et al. Compound Danshen Dripping Pill inhibits hypercholesterolemia/atherosclerosis-induced heart failure in ApoE and LDLR dual deficient mice *via* multiple mechanisms. *Acta Pharm Sin B* 2023;**13**:1036-52.

32 Yang HX, Zhang M, Long SY, Tuo QH, Tian Y, Chen JX, et al. Cholesterol in LDL receptor recycling and degradation. *Clin Chim Acta* 2020;**500**:81-6.

33 Jia Y, Wang B, Wu X, Li S, Hu J, Wang D, et al. Simultaneous quantification of 2′,3′,5′-tri-*O*-acetyl-N^6-(3-hydroxylaniline)adenosine and its principal metabolites in hamster blood by LC–MS/MS and its application in pharmacokinetics study. *J Chromatogr B Analyt Technol Biomed Life Sci* 2016;**1022**:46-53.

34 Liu Y, He J, Abliz Z, Zhu H. *In vitro* stability and metabolism of O2′,O3′,O5′-tri-acetyl-N^6-(3-hydroxylaniline) adenosine in rat, dog and human plasma: chemical hydrolysis and role of plasma esterases. *Xenobiotica* 2011;**41**:549-60.

35 Miao J, Manthena PV, Haas ME, Ling AV, Shin DJ, Graham MJ, et al. Role of insulin in the regulation of proprotein convertase subtilisin/kexin type 9. *Arterioscler Thromb Vasc Biol* 2015;**35**:1589-96.

36 Sorrentino V, Zelcer N. Post-transcriptional regulation of lipoprotein receptors by the E3-ubiquitin ligase inducible degrader of the low-density lipoprotein receptor. *Curr Opin Lipidol* 2012;**23**:213-9.

37 Wang JQ, Lin ZC, Li LL, Zhang SF, Li WH, Liu W, et al. SUMOylation of the ubiquitin ligase IDOL decreases LDL receptor levels and is reversed by SENP1. *J Biol Chem* 2021;**296**:100032.

38 He J, Shangguan X, Zhou W, Cao Y, Zheng Q, Tu J, et al. Glucose limitation activates AMPK coupled SENP1–Sirt3 signalling in mitochondria for T cell memory development. *Nat Commun* 2021;**12**:4371.

39 Zhu M, He J, Xu Y, Zuo Y, Zhou W, Yue Z, et al. AMPK activation coupling SENP1–Sirt3 axis protects against acute kidney injury. *Mol Ther* 2023;**31**:3052-66.

40 Dai W, Xu Y, Mo S, Li Q, Yu J, Wang R, et al. GLUT3 induced by AMPK/CREB1 axis is key for withstanding energy stress and augments the efficacy of current colorectal cancer therapies. *Signal Transduct Target Ther* 2020;**5**:177.

41 Rizzolo D, Kong B, Taylor RE, Brinker A, Goedken M, Buckley B, et al. Bile acid homeostasis in female mice deficient in *Cyp7a1* and *Cyp27a1*. *Acta Pharm Sin B* 2021;**11**:3847-56.

42 Cho SY, Lim S, Ahn KS, Kwak HJ, Park J, Um JY. Farnesol induces mitochondrial/peroxisomal biogenesis and thermogenesis by enhancing the AMPK signaling pathway *in vivo* and *in vitro*. *Pharmacol Res* 2021;**163**:105312.

43 Guo L, Kang JS, Park YH, Je BI, Lee YJ, Kang NJ, et al. *S*-Petasin inhibits lipid accumulation in oleic acid-induced HepG2 cells through activation of the AMPK signaling pathway. *Food Funct* 2020;**11**:5664-73.

44 Bjørklund MM, Hollensen AK, Hagensen MK, Dagnaes-Hansen F, Christoffersen C, Mikkelsen JG, et al. Induction of atherosclerosis in mice and hamsters without germline genetic engineering. *Circ Res* 2014;**114**:1684-9.

45 Tao Y, Lan X, Zhang Y, Fu C, Liu L, Cao F, et al. Biomimetic nanomedicines for precise atherosclerosis theranostics. *Acta Pharm Sin B* 2023;**13**:4442-60.

46 Liu H, Wang H, Li Q, Wang Y, He Y, Li X, et al. LPS adsorption and inflammation alleviation by polymyxin B-modified liposomes for atherosclerosis treatment. *Acta Pharm Sin B* 2023;**13**:3817-33.

47 Bonnet F, Scheen A. Understanding and overcoming metformin gastrointestinal intolerance. *Diabetes Obes Metab* 2017;**19**:473-81.

48 Foretz M, Guigas B, Viollet B. Metformin: update on mechanisms of action and repurposing potential.

Nat Rev Endocrinol 2023;**19**:460-76.

49 Chen M, Luo J, Jiang W, Chen L, Miao L, Han C. Cordycepin: a review of strategies to improve the bioavailability and efficacy. *Phytother Res* 2023;**37**:3839-58.

50 Ashraf SA, Elkhalifa AEO, Siddiqui AJ, Patel M, Awadelkareem AM, Snoussi M, et al. Cordycepin for health and wellbeing: a potent bioactive metabolite of an entomopathogenic cordyceps medicinal fungus and its nutraceutical and therapeutic potential. *Molecules* 2020;**25**:2735.

51 Ma A, Wang J, Yang L, An Y, Zhu H. AMPK activation enhances the anti-atherogenic effects of high density lipoproteins in apoE$^{-/-}$ mice. *J Lipid Res* 2017;**58**:1536-47.

52 Gao F, Qian YJ, Chen FH, Zhu HB. Comparative analysis of stimulation and binding characteristics of adenosine analogs to AMP-activated protein kinase. *J Asian Nat Prod Res* 2019;**21**:916-27.

53 Hong C, Marshall SM, McDaniel AL, Graham M, Layne JD, Cai L, et al. The LXR–Idol axis differentially regulates plasma LDL levels in primates and mice. *Cell Metab* 2014;**20**:910-8.

54 Blom DJ, Hala T, Bolognese M, Lillestol MJ, Toth PD, Burgess L, et al. A 52-week placebo-controlled trial of evolocumab in hyperlipidemia. *N Engl J Med* 2014;**370**:1809-19.

55 Schwartz GG, Steg PG, Szarek M, Bhatt DL, Bittner VA, Diaz R, et al. Alirocumab and cardiovascular outcomes after acute coronary syndrome. *N Engl J Med* 2018;**379**:2097-107.

56 Alabi A, Xia XD, Gu HM, Wang F, Deng SJ, Yang N, et al. Membrane type 1 matrix metalloproteinase promotes LDL receptor shedding and accelerates the development of atherosclerosis. *Nat Commun* 2021;**12**:1889.

57 Grześk G, Dorota B, Wołowiec Ł, Wołowiec A, Osiak J, Kozakiewicz M, et al. Safety of PCSK9 inhibitors. *Biomed Pharmacother* 2022;**156**:113957.

58 Huang L, Fan B, Ma A, Shaul PW, Zhu H. Inhibition of ABCA1 protein degradation promotes HDL cholesterol efflux capacity and RCT and reduces atherosclerosis in mice. *J Lipid Res* 2015;**56**:986-97.

Figure captions

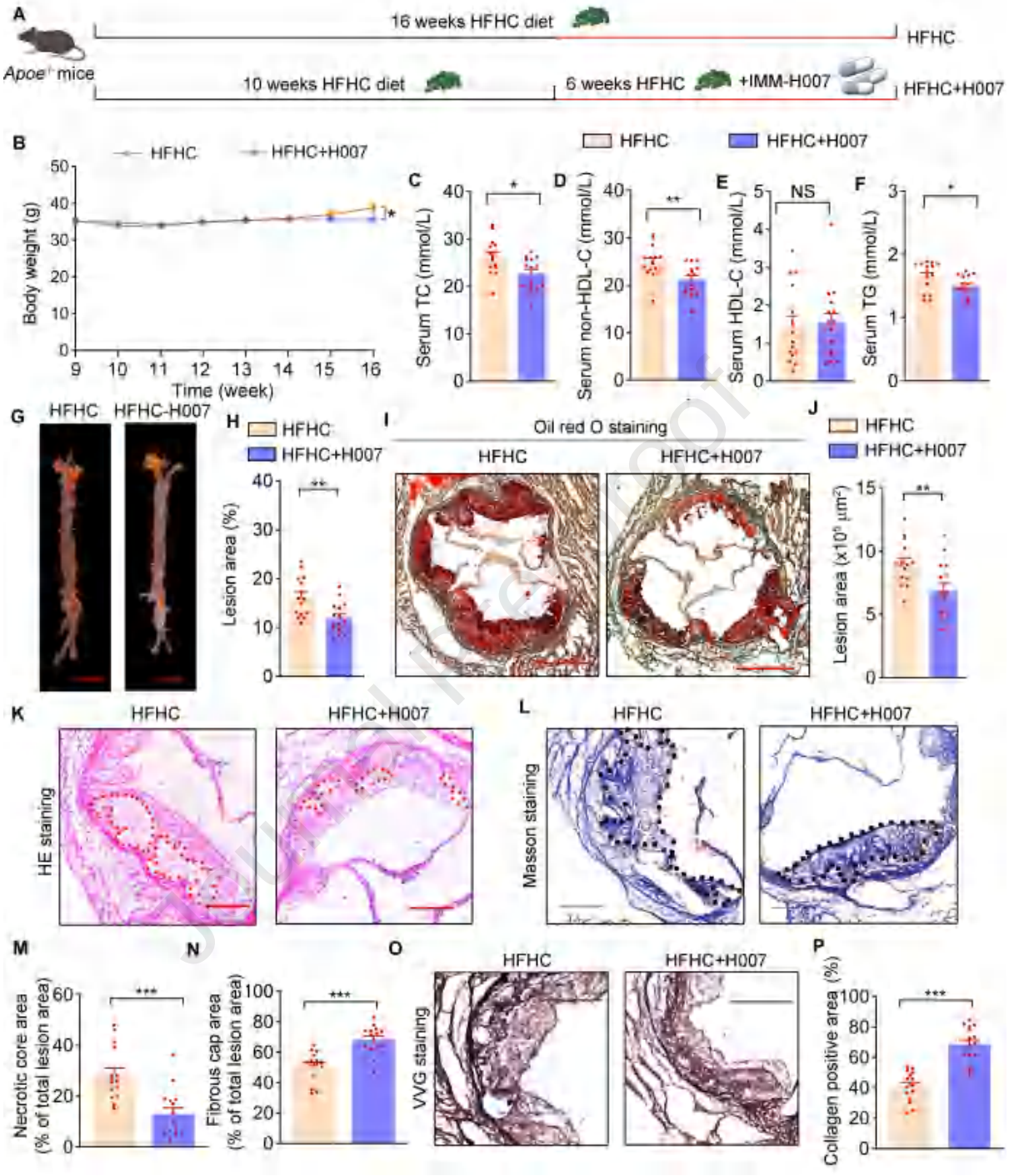

Figure 1 IMM-H007 improves HFHC diet-induced hypercholesterolemia and atherosclerosis in *Apoe*$^{-/-}$ mice. (A) Male apolipoprotein E (*Apoe*)$^{-/-}$ mice (~8 weeks old) were randomly divided into two groups (15 mice/group). In the HFHC group, the mice were fed a high-fat and high-cholesterol diet (HFHC) containing 21% fat plus 0.5% cholesterol for 16 weeks; in the HFHC-H007 group, the mice were fed a HFHC for 10 weeks and then treated with IMM-H007 (200 mg/kg body weight/day) contained in a HFHC for 6 weeks. (B) Body weight from the 9th to the 16th week. (C) Determination of serum total cholesterol (TC). (D) Determination of serum non-high-density lipoprotein-cholesterol (HDL-C). (E) Determination of serum high-density lipoprotein-cholesterol (HDL-C)

levels. (F) Determination of serum triglyceride (TG) levels. (G) *En face* Oil red O (ORO) staining. Scale bar = 5 mm. (H) Lesions in *en face* aortas were quantified *via* a computer-assisted image analysis protocol. The lesion areas are expressed as percentages of the *en face* aorta area. (I) Representative photomicrographs of aortic root sections stained with ORO. Scale bar = 500 μm. (J) Lesions in aortic root cross-sections were quantified *via* a computer-assisted image analysis protocol. The data are expressed as μm^2 in aortic root cross-sections. (K) Representative photomicrographs of aortic root sections stained with hematoxylin and eosin (HE). Necrotic cores are marked by red dashed lines. Scale bar = 200 μm. (L) Representative photomicrographs of aortic root sections stained with Masson staining. Fibrous caps are marked by black dashed lines. Scale bar = 200 μm. (M, N) Quantitative analysis of the necrotic core area (M) and fibrous cap area (N). (O) Representative photomicrographs of aortic root sections stained with Verhoeff–van Gieson (VVG). Scale bar = 250 μm. (P) The collagen-positive areas are expressed as percentages of the aortic area. Statistical data are presented as mean ± SEM. **P* < 0.05; ***P* < 0.01; ****P* < 0.001; NS, not significant *versus* the indicated group (*n* = 15).

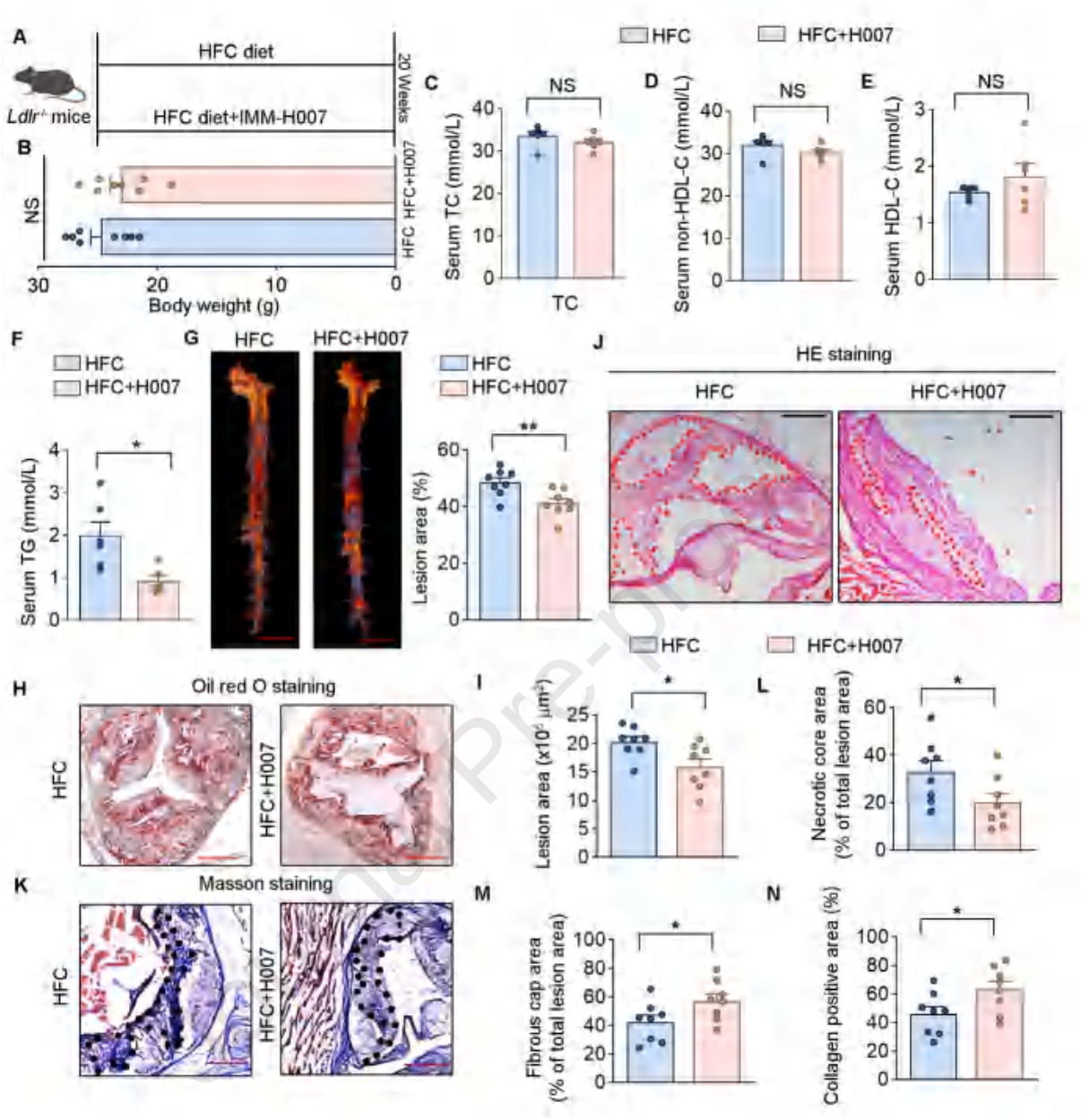

Figure 2 IMM-H007 inhibits atherosclerosis in *Ldlr*$^{-/-}$ mice. (A, B) Male low-density lipoprotein receptor (*Ldlr*)$^{-/-}$ mice were fed high-fat, high-cholesterol (HFC) or HFC containing IMM-H007 (200 mg/kg body weight/day) for 20 weeks (A), and their body weights were measured in the 20th week (B). (C–F) Determination of serum TC (C), non-HDL-C (D), HDL-C (E), and TG (F) levels (n = 6). (G) *En face* lesions were determined by Oil Red O staining and quantified as a percentage (n = 8). Scale bar = 5 mm. (H, I) Aortic root sections were subjected to Oil Red O staining (H), followed by quantification of lesions in the aortic root (I) (n = 8). Scale bar = 500 μm. (J) Aortic root sections were subjected to HE staining. Necrotic cores are marked by red dashed lines. Scale bar = 200 μm. (K) Representative photomicrographs of aortic root sections stained with Masson staining. The fibrous cap is marked by a black dashed line. Scale bar = 250 μm. (L, M) Quantification of lesions in the necrotic core area (L) and fibrous cap area (M) (n = 8). (N) The collagen-positive areas are expressed as percentages of the aortic area (n = 8). Statistical data are

presented as mean±SEM. *$P < 0.05$, **$P < 0.01$; NS, not significant *versus* the indicated group.

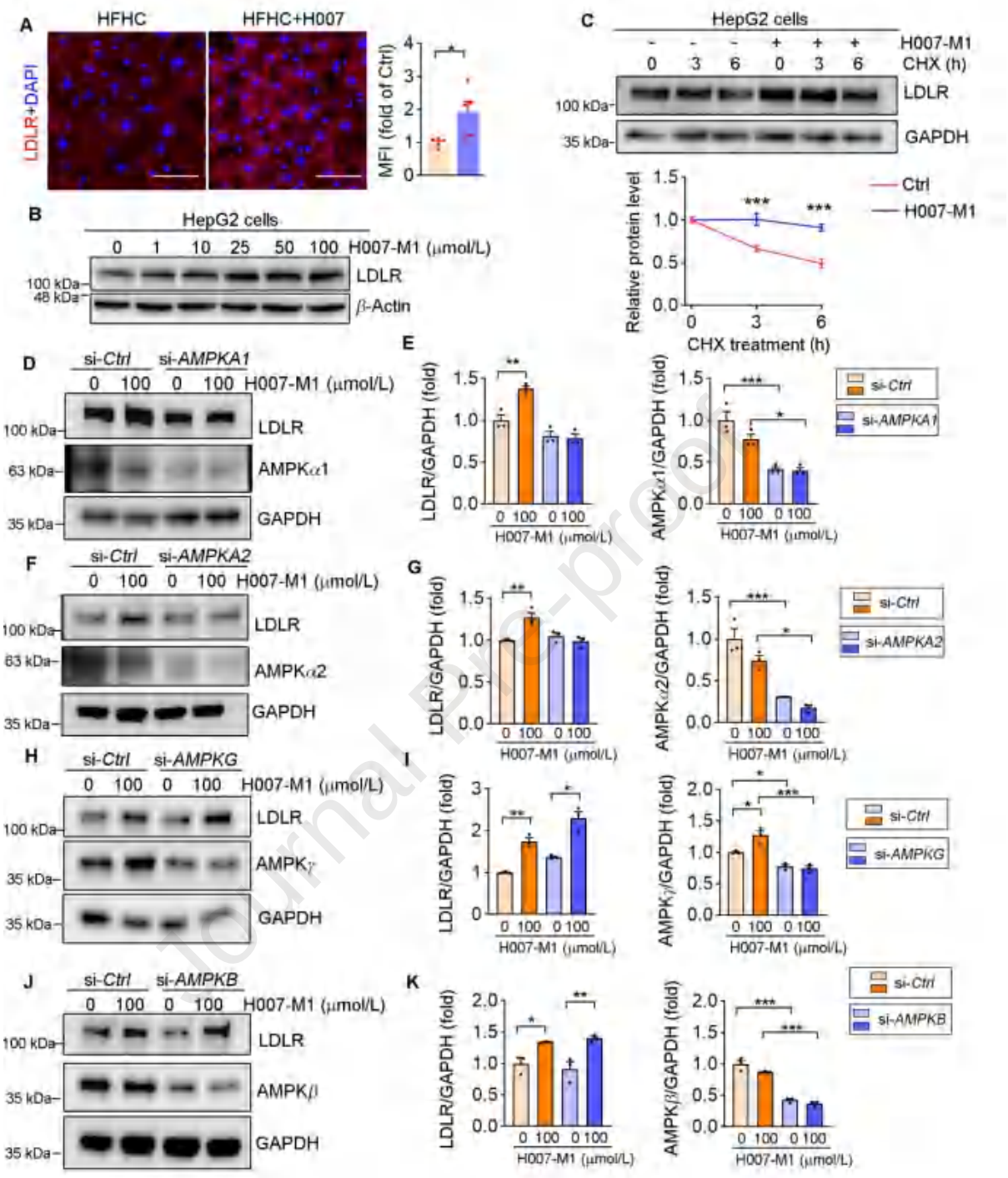

Figure 3 The increase in LDLR protein levels induced by IMM-H007 depends on AMPKα1/2. (A) LDLR protein levels in *Apoe*$^{-/-}$ mouse livers were determined via immunofluorescence staining, and the mean immunofluorescence intensity (MFI) of the images was quantified. Scale bar = 50 μm. n = 5. (B) HepG2 cells were treated with H007-M1 at the indicated concentrations for 24 h. LDLR protein expression was determined by Western blotting. (C) HepG2 cells were pretreated with H007-M1 (100 μmol/L) for 12 h and then incubated with CHX (100 μmol/L) for 0, 3, or 6 h. LDLR protein expression was determined by Western blot (top), and the half-life was calculated (bottom). (D, E) HepG2 cells were transfected with scrambled siRNA or AMP-activated protein kinase (*Ampk*)

*a*1 siRNA and treated with H007-M1 (100 μmol/L) for 24 h. LDLR and AMPK*α*1 protein expression was subsequently determined *via* Western blotting (D), and the band density (E) was quantified. (F, G) HepG2 cells were transfected with scrambled siRNA or *AMPKA*2 siRNA and treated with H007-M1 (100 μmol/L) for 24 h, after which LDLR and AMPK*α*2 protein expression was determined by Western blotting (F), and the band density was quantified (G). (H, I) HepG2 cells were transfected with scrambled siRNA or *AMPKG* siRNA and treated with H007-M1 (100 μmol/L) for 24 h, after which LDLR and AMPK*γ* protein expression was determined by Western blotting (H), and the band density was quantified (I). (J, K) HepG2 cells were transfected with scrambled siRNA or *AMPKB* siRNA and treated with H007-M1 (100 μmol/L) for 24 h. LDLR and AMPK*β* protein expression levels were subsequently determined *via* Western blotting (J), and the band density (K) was quantified. Statistical data are presented as mean±SEM. **P* < 0.05; ***P* < 0.01; ****P* < 0.001 *versus* the indicated group (*n* = 3).

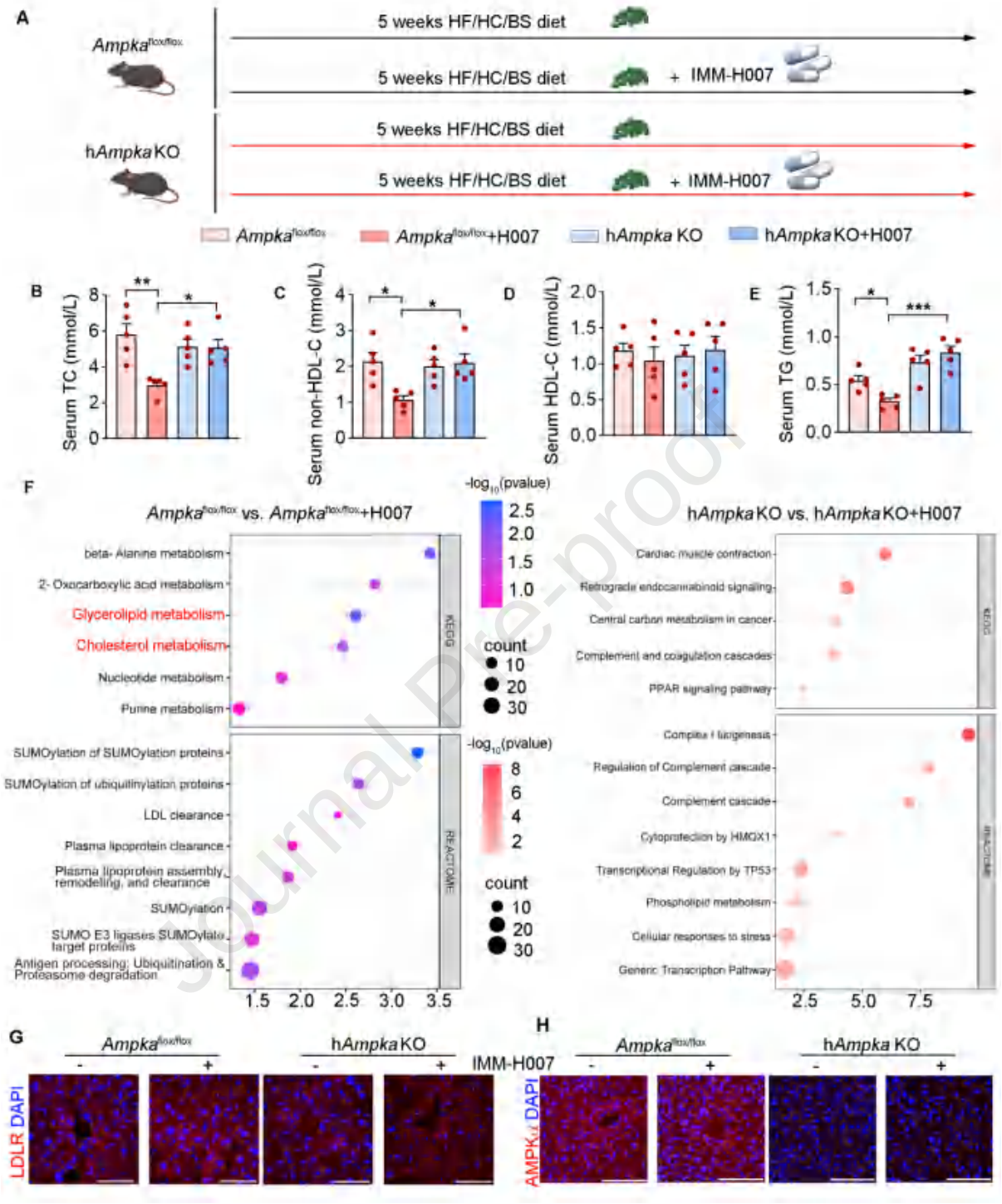

Figure 4 Hepatocyte *Ampka*1/2 deficiency blocked the effect of IMM-H007 on hypercholesterolemia. (A) *Ampka*$^{flox/flox}$ and h*Ampka* KO mice were fed a high-fat (HF)/high-cholesterol (HC)/bile-salt (BS) diet with or without IMM-H007 (200 mg/kg body weight/day) for 5 weeks. (B) Determination of serum TC. (C) Determination of non-HDL-C. (D) Determination of HDL-C levels. (E) Determination of serum TG levels. Statistical data are presented as mean±SEM. **P* < 0.05; ***P* < 0.01; ****P* < 0.001 *versus* the indicated group (*n* = 5). (F) RNA-seq assay with mouse liver total RNA. Enrichment analysis of the KEGG and REACTOME pathways (*n* = 3). (G,

H) Protein levels of LDLR (G, scale bar = 100 μm) AMPKα1/2 (H, scale bar = 200 μm) in mouse liver was determined by immunofluorescent staining.

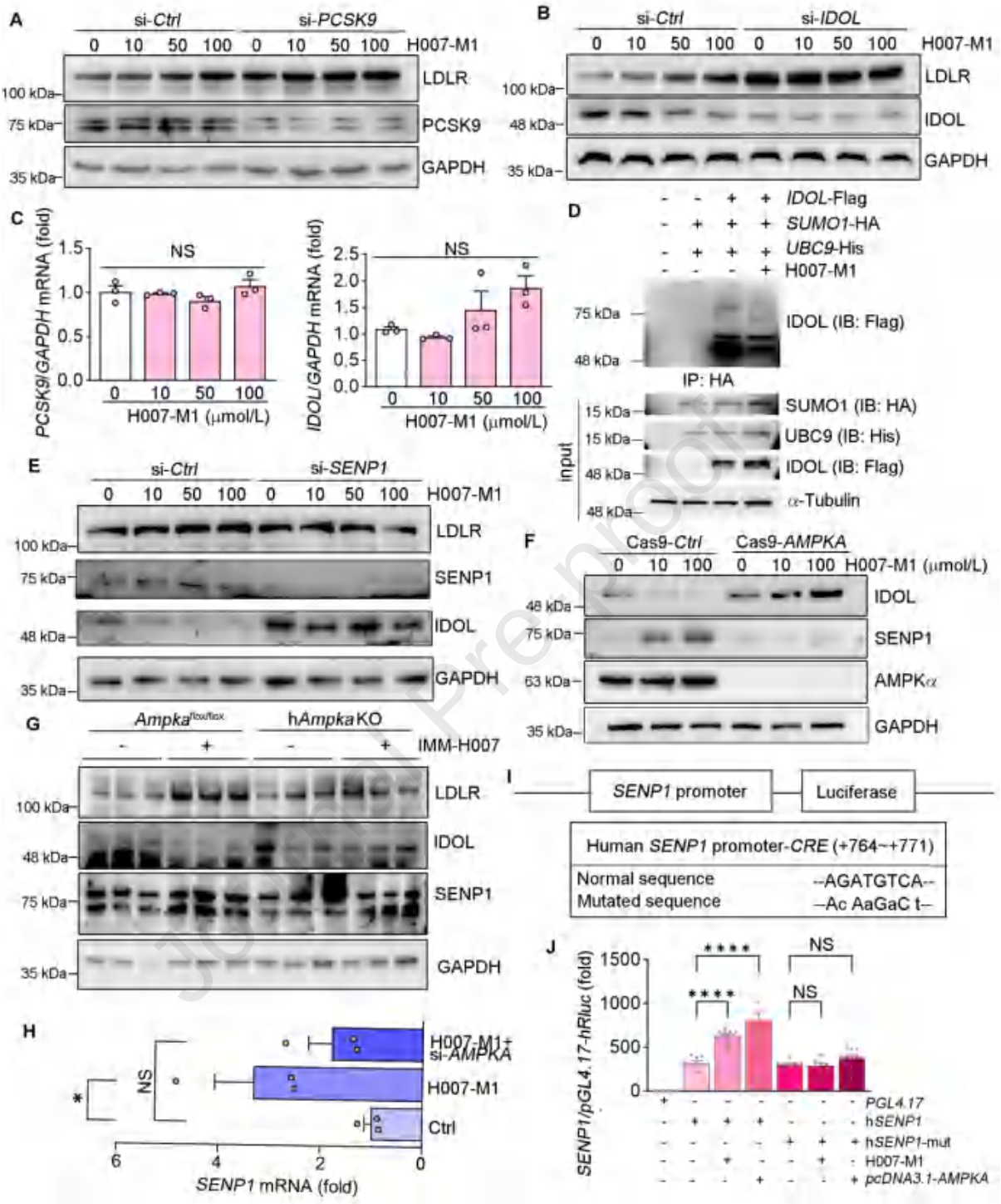

Figure 5 IMM-H007 upregulates LDLR expression *via* the AMPKα1/2–SENP1–IDOL signaling pathway. (A, B) HepG2 cells were posttranslationally transfected with scrambled siRNA, proprotein convertase subtilisin/kexin type 9 (*PCSK9*) siRNA (A), or inducible degrader of LDLR (*IDOL*) siRNA (B), after which LDLR, PCSK9, and IDOL protein expression was determined by Western blotting. (C) mRNA levels of *PCSK9* and *IDOL* in HepG2 cells after H007-M1 treatment were measured *via* qRT-PCR (n = 3). (D) HEK-293T cells were transfected with Flag-*IDOL*, HA-small ubiquitin-like modifier 1 (*SUMO1*), or His-ubiquitin-conjugating enzyme (*UBC9*) for 24 h and then treated with H007-M1 (100 μmol/L) for 24 h. The SUMOylation of Flag-*IDOL* was determined by

an IP assay using Flag beads. (E) HepG2 cells were transfected with scrambled siRNA or SUMO-specific protease 1 (*SENP1*) siRNA, after which the protein expression of IDOL, SENP1, and LDLR was determined by Western blotting. (F) Cas9-Ctrl and Cas9-*AMPKA* cells were treated with H007-M1 at the indicated concentrations for 24 h. IDOL, SENP1, and AMPKA protein expression was determined by Western blotting. (G) Protein expression in the livers of the mice in Fig. 4A was determined by Western blotting. (H) mRNA levels of *SENP1* in HepG2 cells after H007-M1 treatment or transfection with *AMPKA*1/2 siRNA were measured *via* qRT-PCR (n = 3). (I) Putative cAMP response element (*CRE)* region in the h*SENP1* promoter and the mutated sites. (J) HepG2 cells were transfected with the *SENP1* promoter or *SENP1-CRE*-mut promoter and *Renilla* (as an internal control) overnight, followed by 100 μmol/L H007-M1 treatment or *AMPKA*1/2 overexpression for another 24 h. The activity of firefly and *Renilla* luciferases in the cellular lysate was determined *via* a dual-luciferase reporter assay (n = 8). Statistical data are presented as mean± SEM. **P < 0.01; ***P < 0.001; ****P < 0.0001; NS, not significant *versus* the indicated groups.

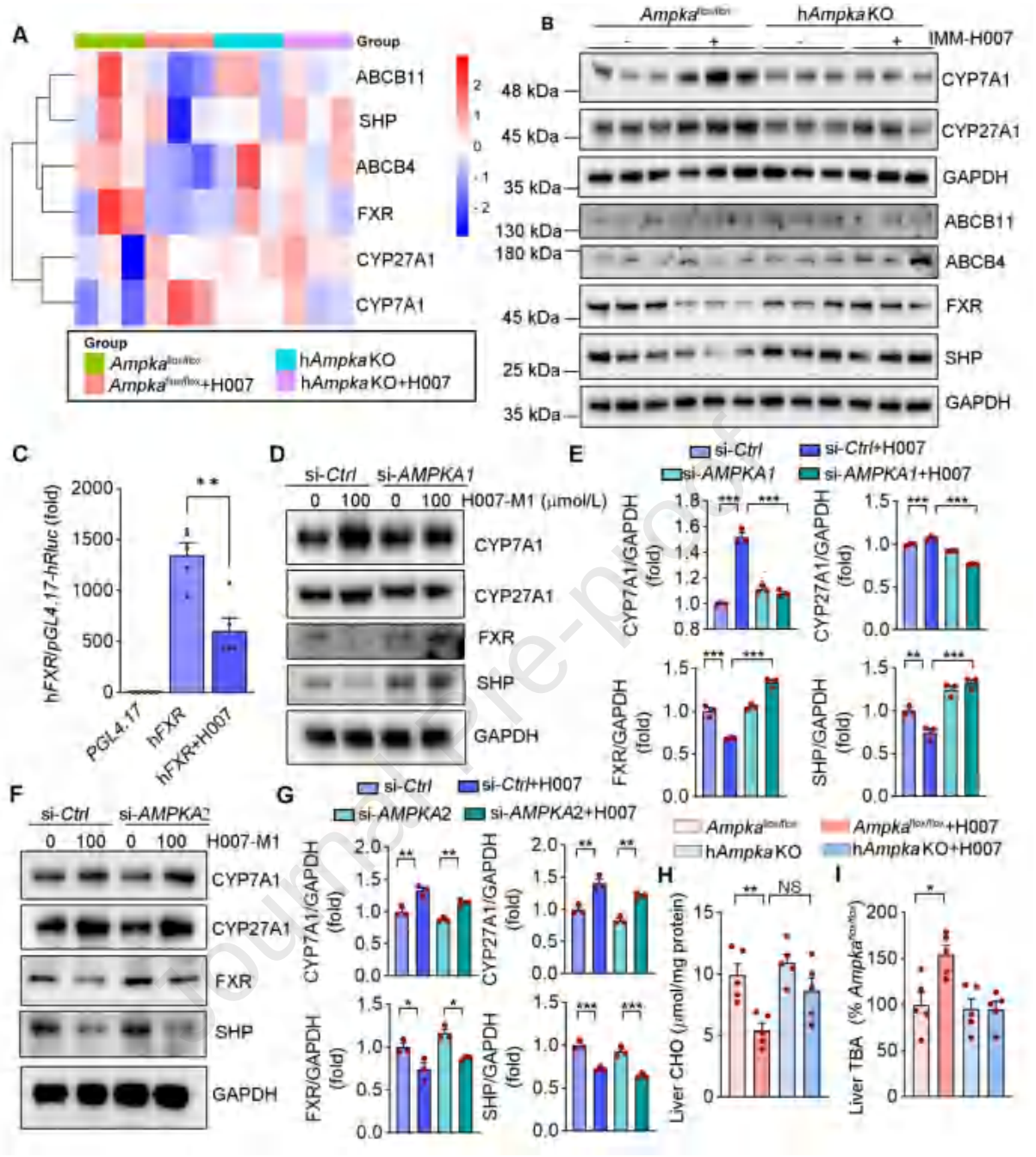

Figure 6 IMM-H007 promotes hepatic cholesterol metabolism by activating the AMPKα1–FXR pathway. (A) Heatmap of the differentially expressed genes related to bile acid metabolism in the liver identified *via* RNA-seq. (B) Cholesterol metabolism-related protein expression in the livers of the mice shown in Fig. 4A was determined by Western blotting. (C) 293T cells were transfected with the farnesoid X receptor (*FXR*) promoter and *Renilla* (as an internal control) overnight, followed by 100 μmol/L H007-M1 treatment for another 24 h. The activity of firefly and *Renilla* luciferases in the cellular lysate was determined *via* a dual-luciferase reporter assay (n = 5). (D, E) HepG2 cells were transfected with scrambled siRNA or *AMPKA1* siRNA and treated with H007-M1 (100 μmol/L) for 24 h. Then, protein expression was determined by Western blotting (D), and the band density (E) was quantified. (F, G) HepG2 cells were transfected with scrambled siRNA or

AMPKA2 siRNA and treated with H007-M1 (100 μmol/L) for 24 h. Then, protein expression was determined by Western blotting (F), and the band density was quantified (G) (n = 3). (H) Hepatic cholesterol quantitative analysis of the mice in Fig. 4A. (I) Hepatic total bile acid (TBA) quantitative analysis of the mice in Fig. 4A (n = 5). Statistical data are presented as mean±SEM. *P < 0.05; **P < 0.01; ***P < 0.001; NS, not significant *versus* the indicated group.

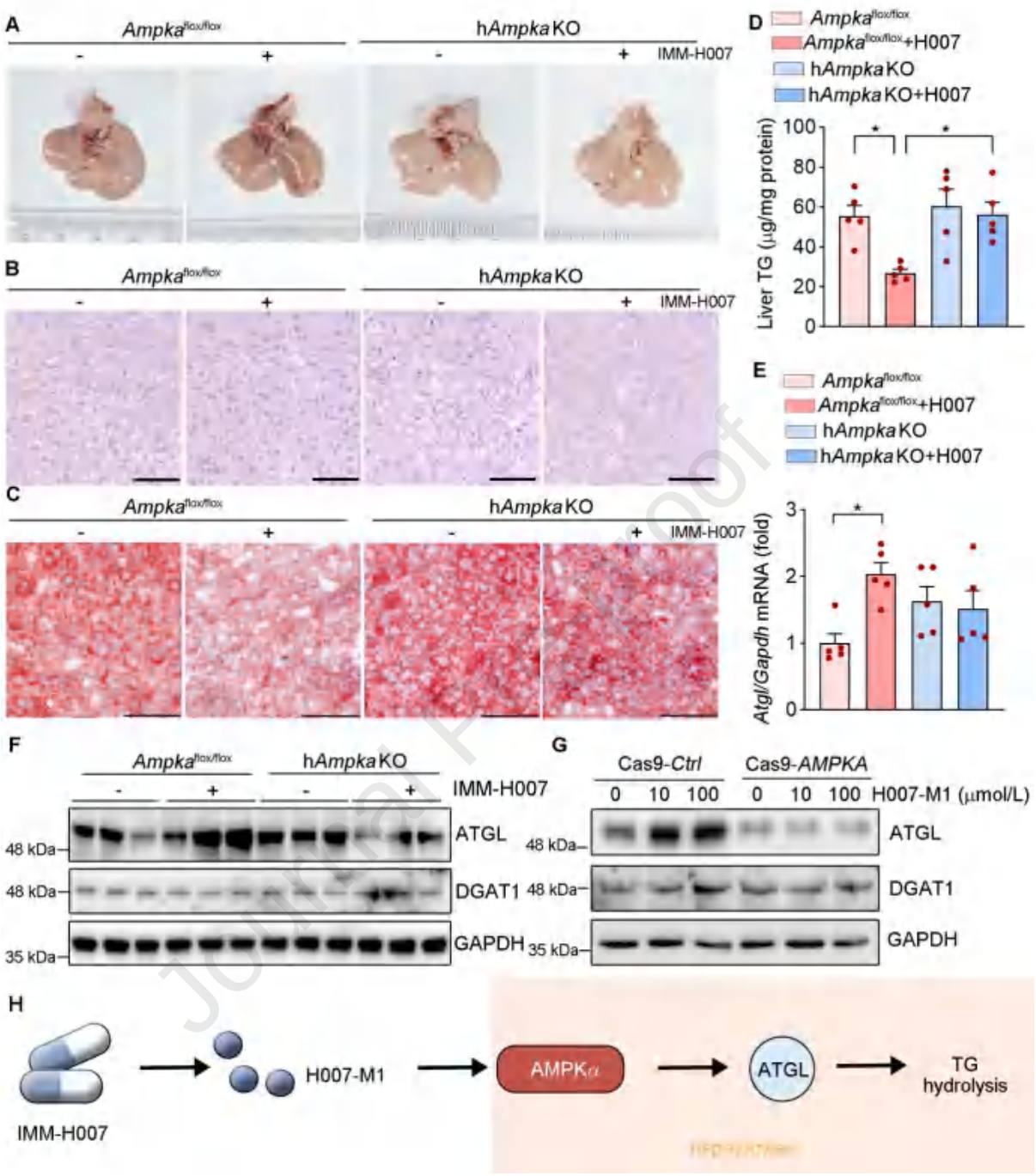

Figure 7 Hepatocyte *AMPKα*1/2 deficiency increases lipid accumulation in the liver. (A) Liver photos of the mice in Fig. 4A. (B, C) HE (B) and ORO (C) staining of liver sections from the mice in Fig. 4A. Scale bar = 100 μm. (D) TG quantitative analysis of total liver lipid extracts from the mice in Fig. 2A (n = 5). (E) Adipose triglyceride lipase (*ATGL*) mRNA expression in the livers of the mice shown in Fig. 4A was determined by qRT-PCR (n = 5). (F) ATGL, diacylglycerol *O*-acyltransferase 1 (DGAT1) protein expression in the livers of the mice in Fig. 4A was determined by Western blotting (n = 3). (G) Cas9-Ctrl and Cas9-*AMPKA* HepG2 cells were treated with H007-M1 at the indicated concentrations for 12 h. Protein expression was determined by Western blotting (n = 3). (H) Schematic diagram of the potential mechanism by which IMM-H007 decreases hepatic

lipid accumulation. Statistical data are presented as mean±SEM. *$P < 0.05$ *versus* the indicated groups.

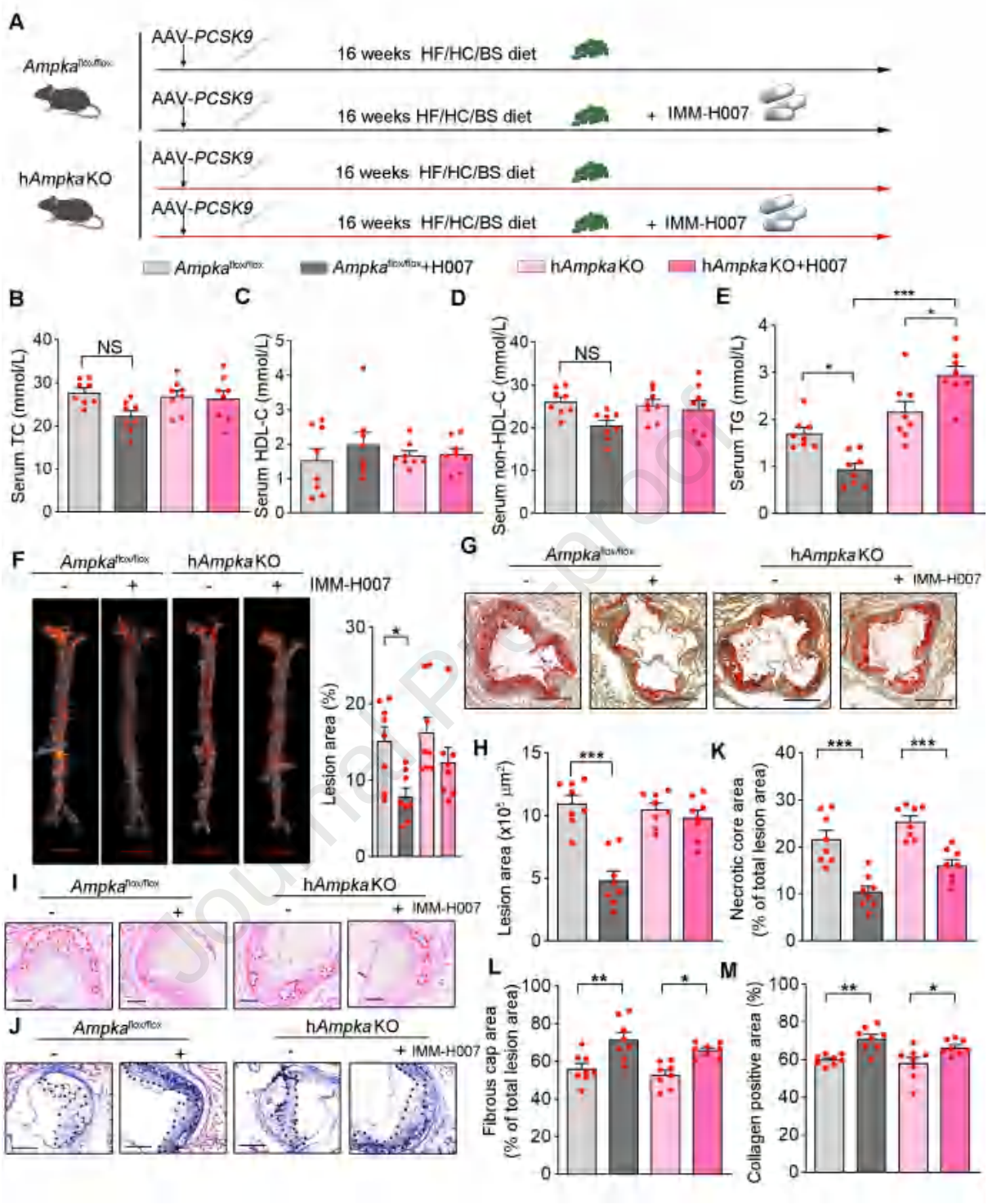

Figure 8 Hepatocyte *Ampka*1/2 deficiency blocked the effect of IMM-H007 on atherosclerosis. (A) *Ampka*$^{flox/flox}$ and h*Ampka* KO mice were administered AAV-*PCSK9* through the tail vein. Subsequently, they were fed a HF/HC/BS diet for 16 weeks, with two groups receiving IMM-H007 (200 mg/kg body weight/day). (B) Determination of serum TC. (C) Determination of HDL-C. (D) Determination of non-HDL-C levels. (E) Determination of serum TG levels. (F) *En face* ORO staining and quantification via a computer-assisted image analysis protocol. The lesion areas are expressed as percentages of the *en face* aorta area. Scale bar = 5 mm. (G) Representative

photomicrographs of aortic root sections stained with ORO. Scale bar = 500 μm. (H) Lesions in aortic root cross-sections were quantified *via* a computer-assisted image analysis protocol. The lesion areas are expressed as μm^2 in aortic root cross-sections. (I) Representative photomicrographs of aortic root sections stained with HE. Necrotic cores are marked by red dashed lines. Scale bar = 200 μm. (J) Representative photomicrographs of aortic root sections stained with Masson staining. Fibrous caps are marked by black dashed lines. Scale bar = 200 μm. (K, L) Masson staining followed by quantitative analysis of the necrotic core area (K) and fibrous cap area (L). (M) The collagen-positive areas are expressed as percentages of the aortic area (n = 8). Statistical data are presented as mean±SEM. *$P < 0.05$; **$P < 0.01$; ***$P < 0.001$; NS, not significant *versus* the indicated group.

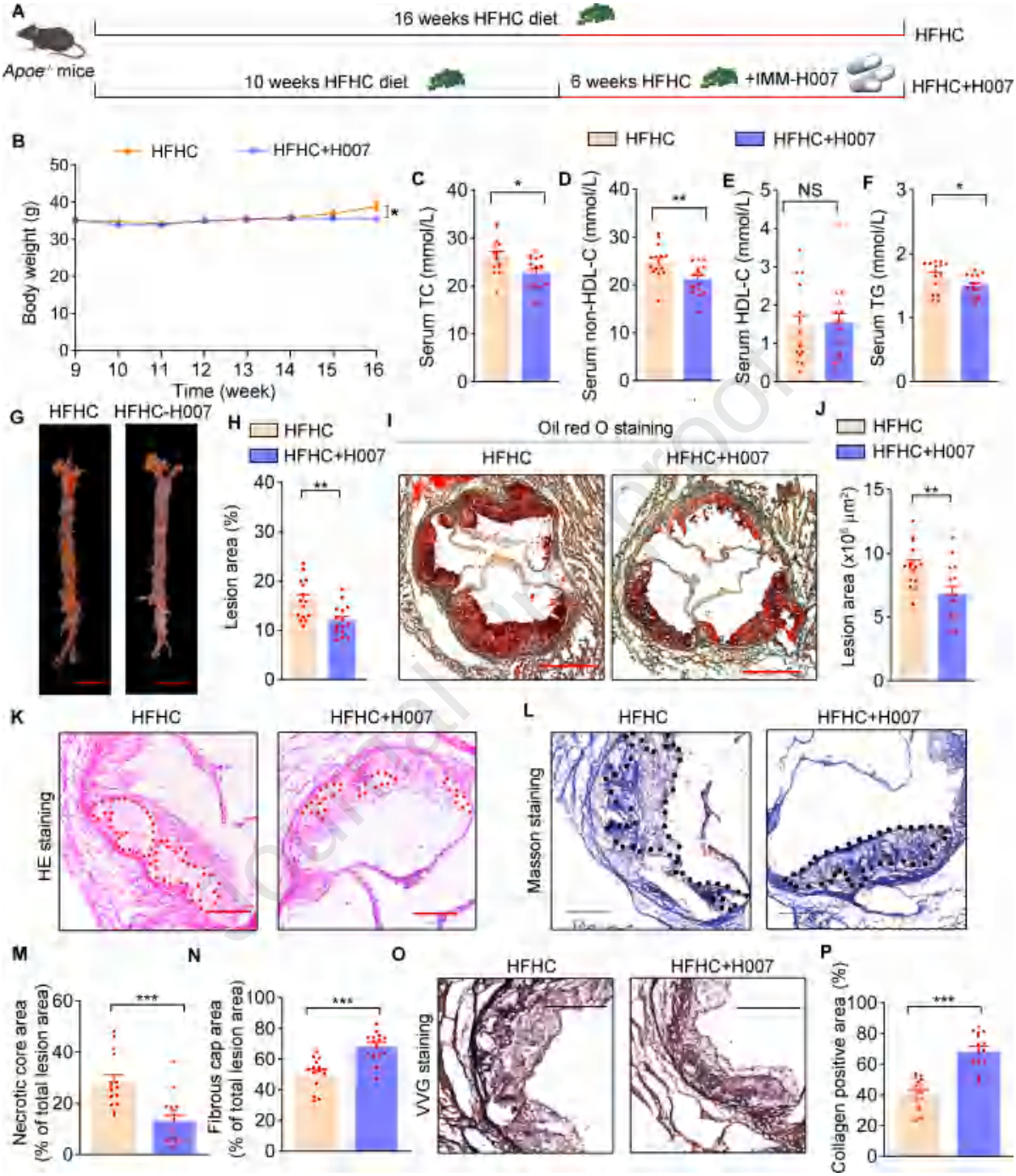
A
16 weeks HFHC diet
HFHC
Apoe-/- mice
10 weeks HFHC diet
6 weeks HFHC
+IMM-H007
HFHC+H007
B
HFHC
HFHC+H007
Body weight (g)
Time (week)
C
Serum TC (mmol/L)
D
Serum non-HDL-C (mmol/L)
E
Serum HDL-C (mmol/L)
NS
F
Serum TG (mmol/L)
G
HFHC
HFHC-H007
H
Lesion area (%)
I
Oil red O staining
HFHC
HFHC+H007
J
Lesion area (x10³ μm²)
K
HE staining
L
Masson staining
M
Necrotic core area (% of total lesion area)
N
Fibrous cap area (% of total lesion area)
O
VVG staining
P
Collagen positive area (%)

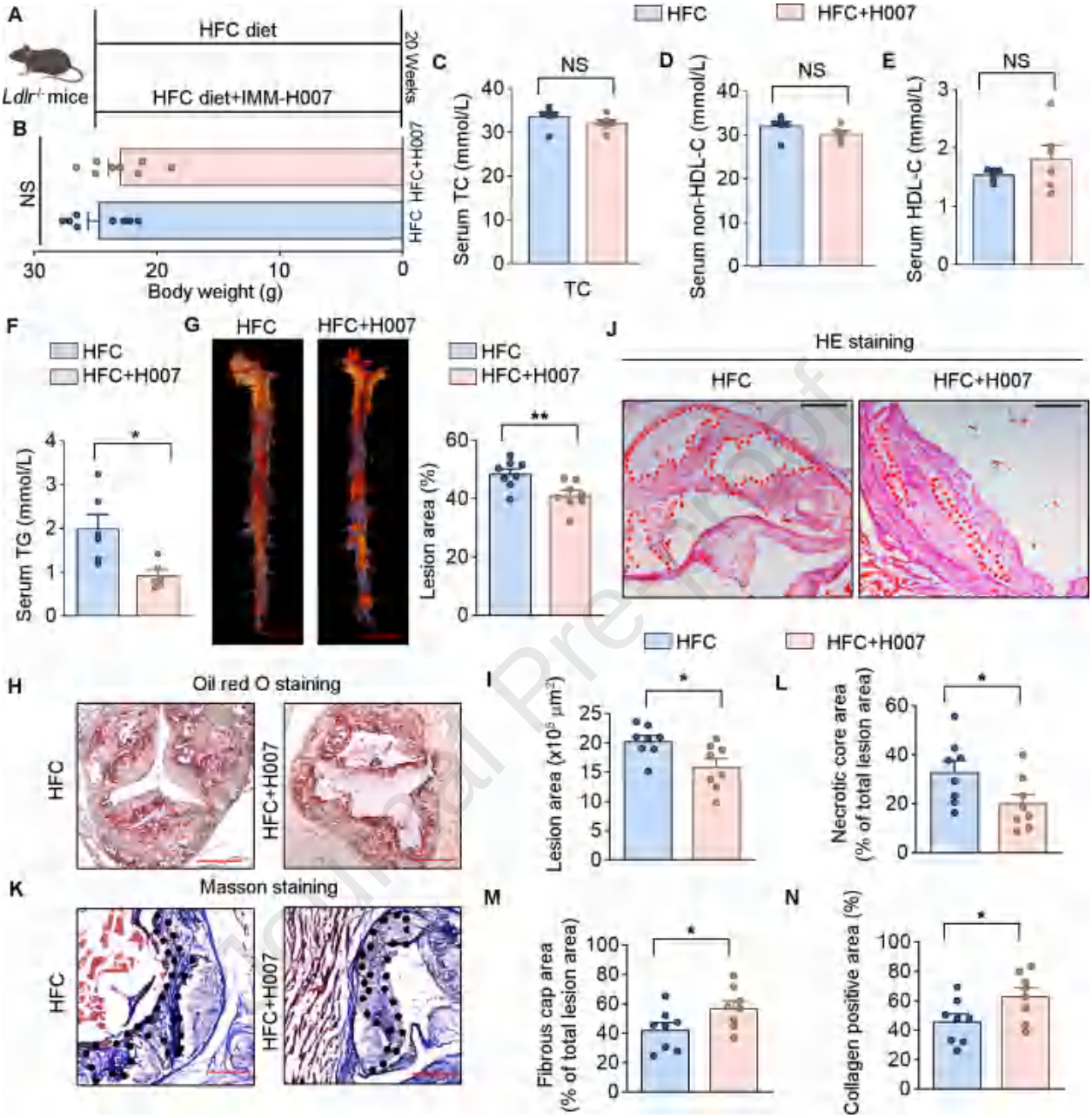
A
HFC diet
HFC diet+IMM-H007
Ldlr-/- mice
20 Weeks
B
NS
HFC
HFC+H007
30
20
10
0
Body weight (g)
HFC
HFC+H007
C
NS
Serum TC (mmol/L)
TC
D
NS
Serum non-HDL-C (mmol/L)
E
NS
Serum HDL-C (mmol/L)
F
HFC
HFC+H007
*
Serum TG (mmol/L)
G
HFC
HFC+H007
HFC
HFC+H007
**
Lesion area (%)
J
HE staining
HFC
HFC+H007
H
Oil red O staining
HFC
HFC+H007
I
HFC
HFC+H007
*
Lesion area (x10^5 μm^2)
L
*
Necrotic core area (% of total lesion area)
K
Masson staining
HFC
HFC+H007
M
*
Fibrous cap area (% of total lesion area)
N
*
Collagen positive area (%)

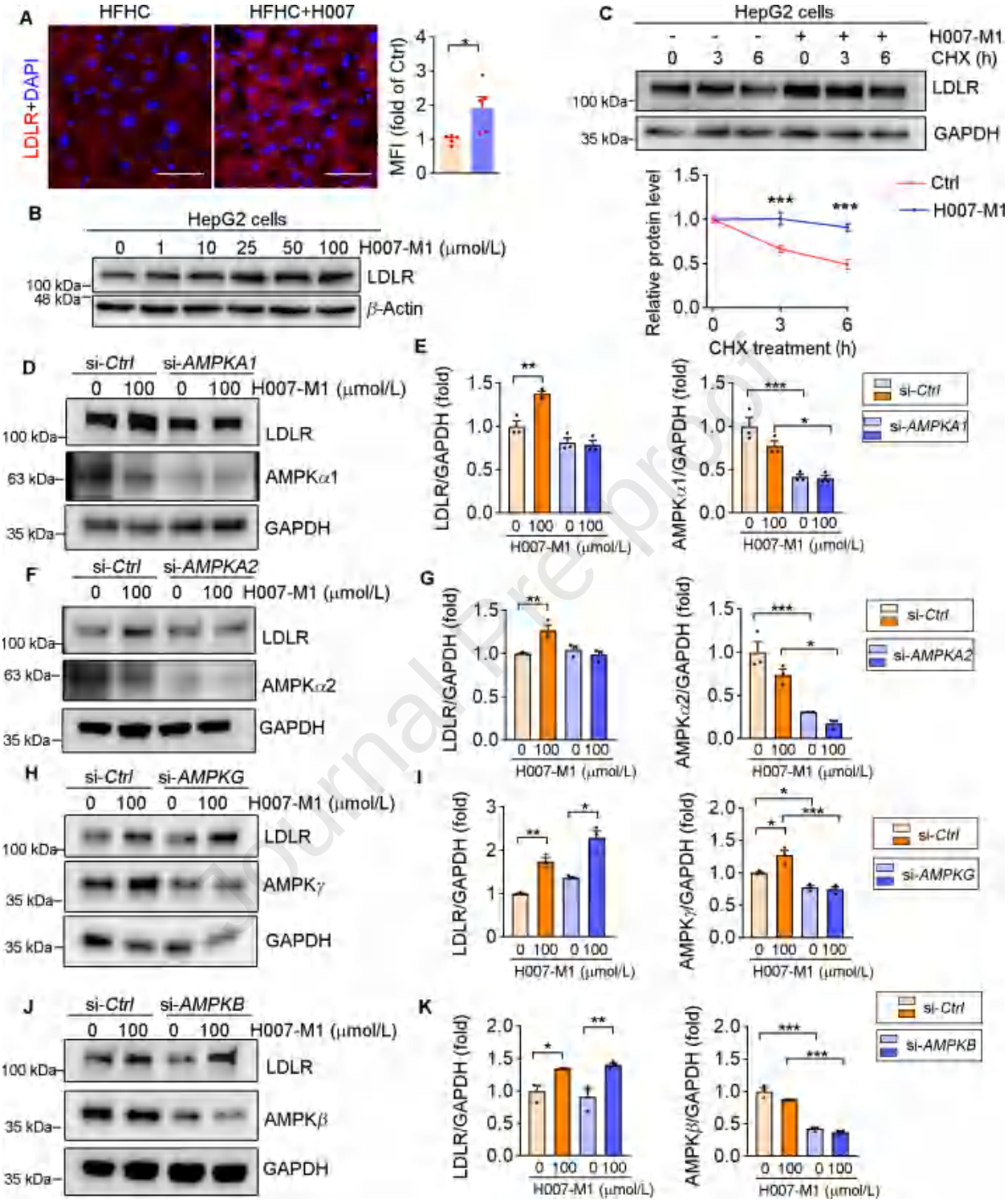
A
HFHC
HFHC+H007
LDLR+DAPI
MFI (fold of Ctrl)
B
HepG2 cells
0 1 10 25 50 100 H007-M1 (μmol/L)
100 kDa
48 kDa
LDLR
β-Actin
C
HepG2 cells
H007-M1
CHX (h)
100 kDa
35 kDa
LDLR
GAPDH
Relative protein level
CHX treatment (h)
Ctrl
H007-M1
D
si-Ctrl
si-AMPKA1
H007-M1 (μmol/L)
63 kDa
AMPKα1
E
LDLR/GAPDH (fold)
AMPKα1/GAPDH (fold)
F
si-AMPKA2
AMPKα2
G
AMPKα2/GAPDH (fold)
H
si-AMPKG
AMPKγ
I
AMPKγ/GAPDH (fold)
J
si-AMPKB
AMPKβ
K
AMPKβ/GAPDH (fold)

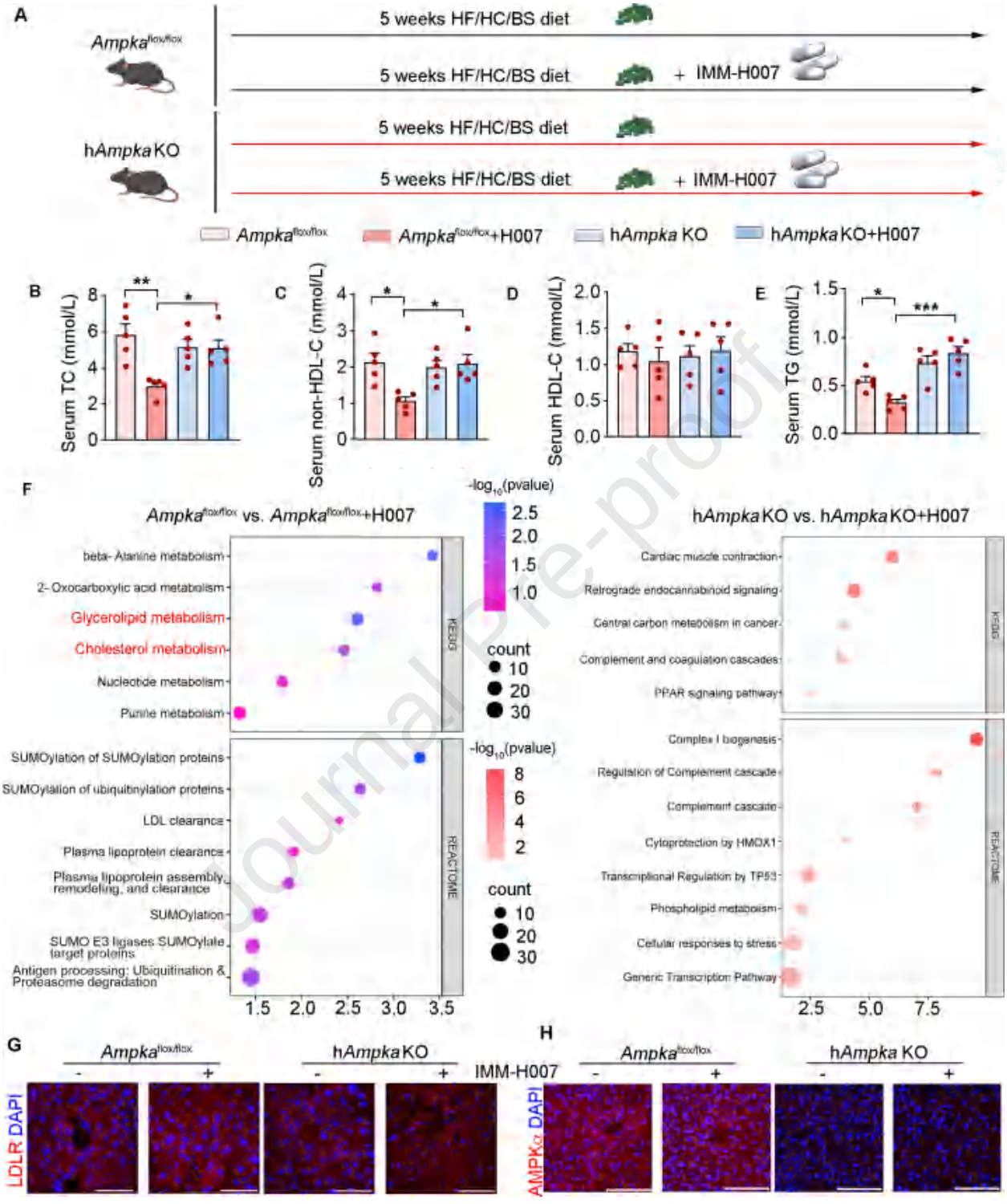

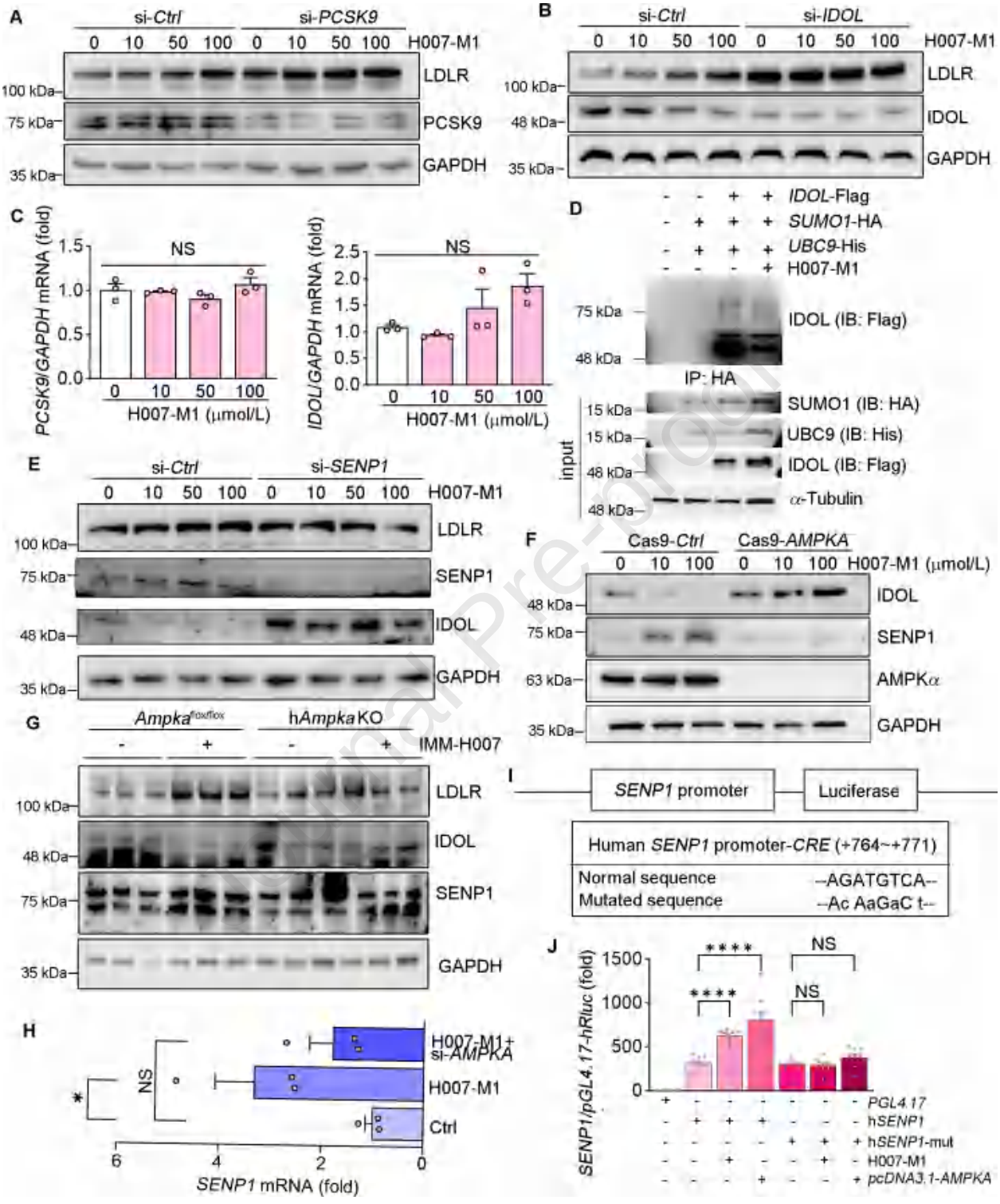
A
si-Ctrl
si-PCSK9
0 10 50 100 0 10 50 100 H007-M1
100 kDa
75 kDa
35 kDa
LDLR
PCSK9
GAPDH
B
si-Ctrl
si-IDOL
0 10 50 100 0 10 50 100 H007-M1
100 kDa
48 kDa
35 kDa
LDLR
IDOL
GAPDH
C
PCSK9/GAPDH mRNA (fold)
NS
0 10 50 100
H007-M1 (μmol/L)
IDOL/GAPDH mRNA (fold)
NS
0 10 50 100
H007-M1 (μmol/L)
D
IDOL-Flag
SUMO1-HA
UBC9-His
H007-M1
75 kDa
48 kDa
IDOL (IB: Flag)
IP: HA
15 kDa
15 kDa
48 kDa
48 kDa
SUMO1 (IB: HA)
UBC9 (IB: His)
IDOL (IB: Flag)
α-Tubulin
input
E
si-Ctrl
si-SENP1
0 10 50 100 0 10 50 100 H007-M1
100 kDa
75 kDa
48 kDa
35 kDa
LDLR
SENP1
IDOL
GAPDH
F
Cas9-Ctrl
Cas9-AMPKA
0 10 100 0 10 100 H007-M1 (μmol/L)
48 kDa
75 kDa
63 kDa
35 kDa
IDOL
SENP1
AMPKα
GAPDH
G
Ampkaflox/flox
hAmpkaKO
- + - + IMM-H007
100 kDa
48 kDa
75 kDa
35 kDa
LDLR
IDOL
SENP1
GAPDH
H
H007-M1+ si-AMPKA
H007-M1
Ctrl
NS
*
6 4 2 0
SENP1 mRNA (fold)
I
SENP1 promoter
Luciferase
Human SENP1 promoter-CRE (+764~+771)
Normal sequence --AGATGTCA--
Mutated sequence --Ac AaGaC t--
J
SENP1/pGL4.17-hRluc (fold)
1500
1000
500
0
****
****
NS
NS
PGL4.17
hSENP1
hSENP1-mut
H007-M1
pcDNA3.1-AMPKA

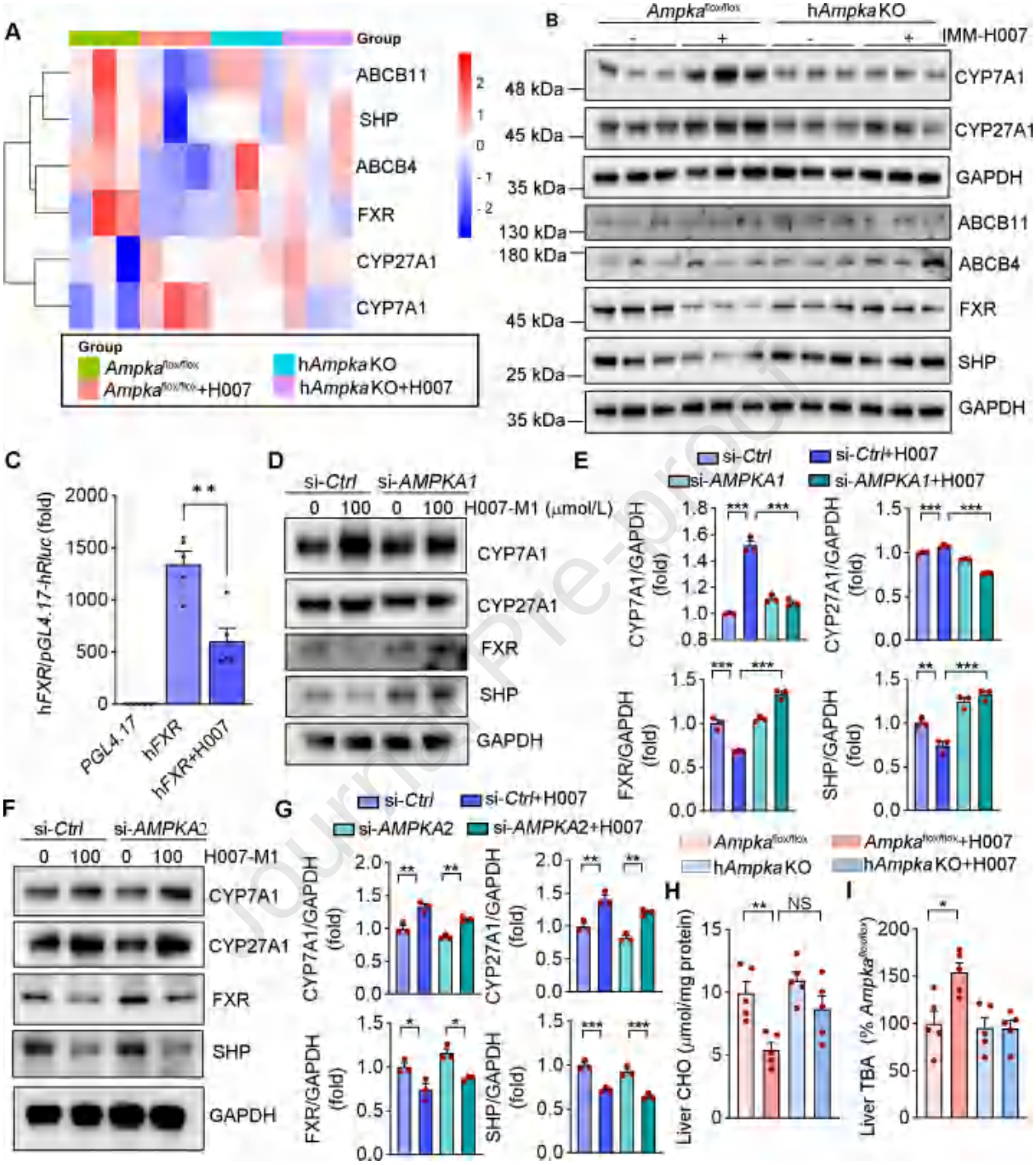
A
Group
ABCB11
SHP
ABCB4
FXR
CYP27A1
CYP7A1
Group
Ampkaflox/flox
Ampkaflox/flox+H007
hAmpkaKO
hAmpkaKO+H007
B
Ampkaflox/flox
hAmpkaKO
IMM-H007
48 kDa
45 kDa
35 kDa
130 kDa
180 kDa
45 kDa
25 kDa
35 kDa
CYP7A1
CYP27A1
GAPDH
ABCB11
ABCB4
FXR
SHP
GAPDH
C
hFXR/pGL4.17-hRluc (fold)
PGL4.17
hFXR
hFXR+H007
D
si-Ctrl
si-AMPKA1
H007-M1 (μmol/L)
CYP7A1
CYP27A1
FXR
SHP
GAPDH
E
si-Ctrl
si-Ctrl+H007
si-AMPKA1
si-AMPKA1+H007
CYP7A1/GAPDH (fold)
CYP27A1/GAPDH (fold)
FXR/GAPDH (fold)
SHP/GAPDH (fold)
F
si-Ctrl
si-AMPKA2
H007-M1
CYP7A1
CYP27A1
FXR
SHP
GAPDH
G
si-Ctrl
si-Ctrl+H007
si-AMPKA2
si-AMPKA2+H007
CYP7A1/GAPDH (fold)
CYP27A1/GAPDH (fold)
FXR/GAPDH (fold)
SHP/GAPDH (fold)
Ampkaflox/flox
Ampkaflox/flox+H007
hAmpkaKO
hAmpkaKO+H007
H
Liver CHO (μmol/mg protein)
NS
I
Liver TBA (% Ampkaflox/flox)

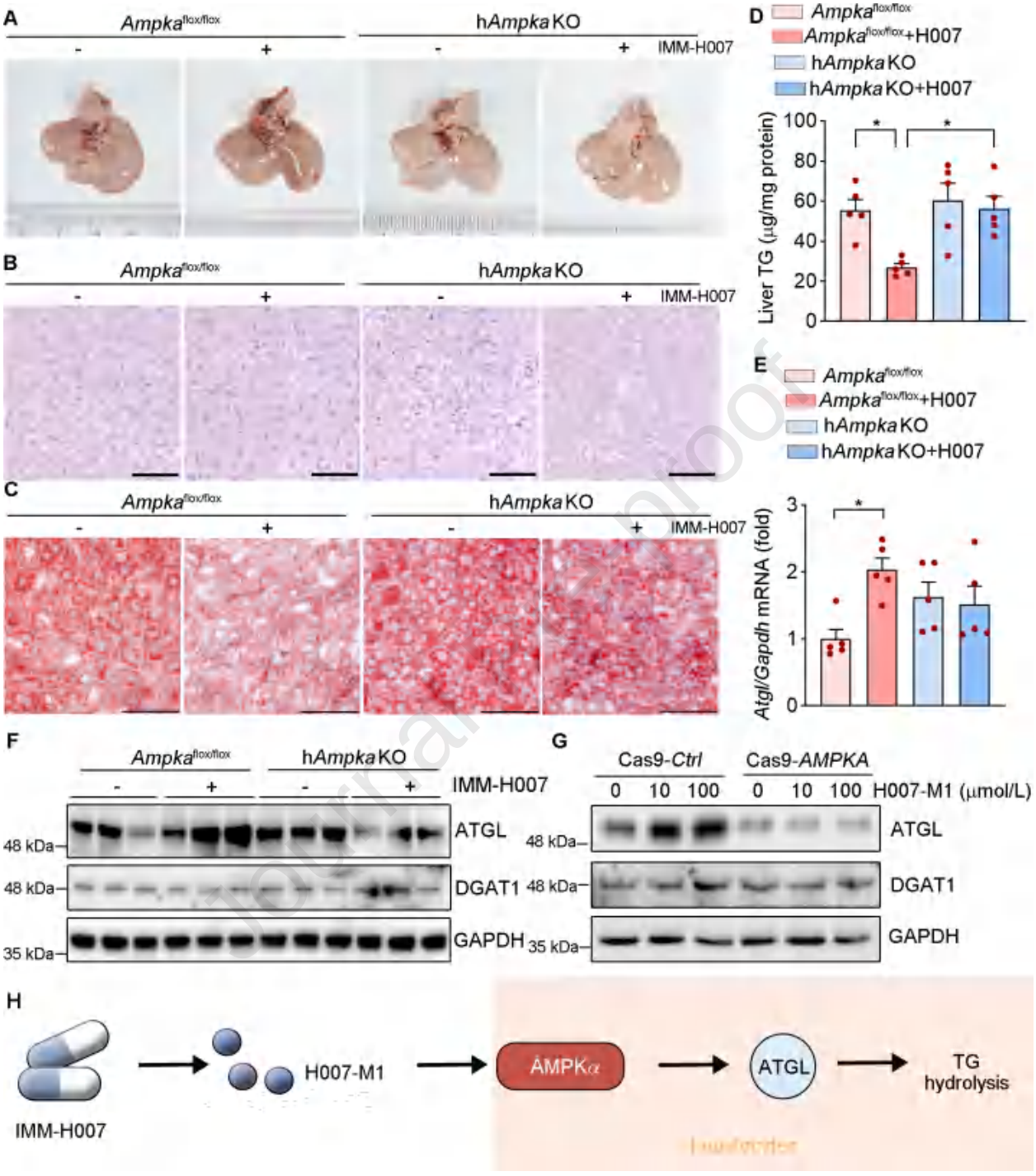
A
Ampkaflox/flox
hAmpkaKO
IMM-H007
B
C
D
Ampkaflox/flox
Ampkaflox/flox+H007
hAmpkaKO
hAmpkaKO+H007
Liver TG (μg/mg protein)
E
Atgl/Gapdh mRNA (fold)
F
48 kDa
ATGL
DGAT1
35 kDa
GAPDH
G
Cas9-Ctrl
Cas9-AMPKA
0 10 100 0 10 100 H007-M1 (μmol/L)
H
H007-M1
AMPKα
ATGL
TG hydrolysis

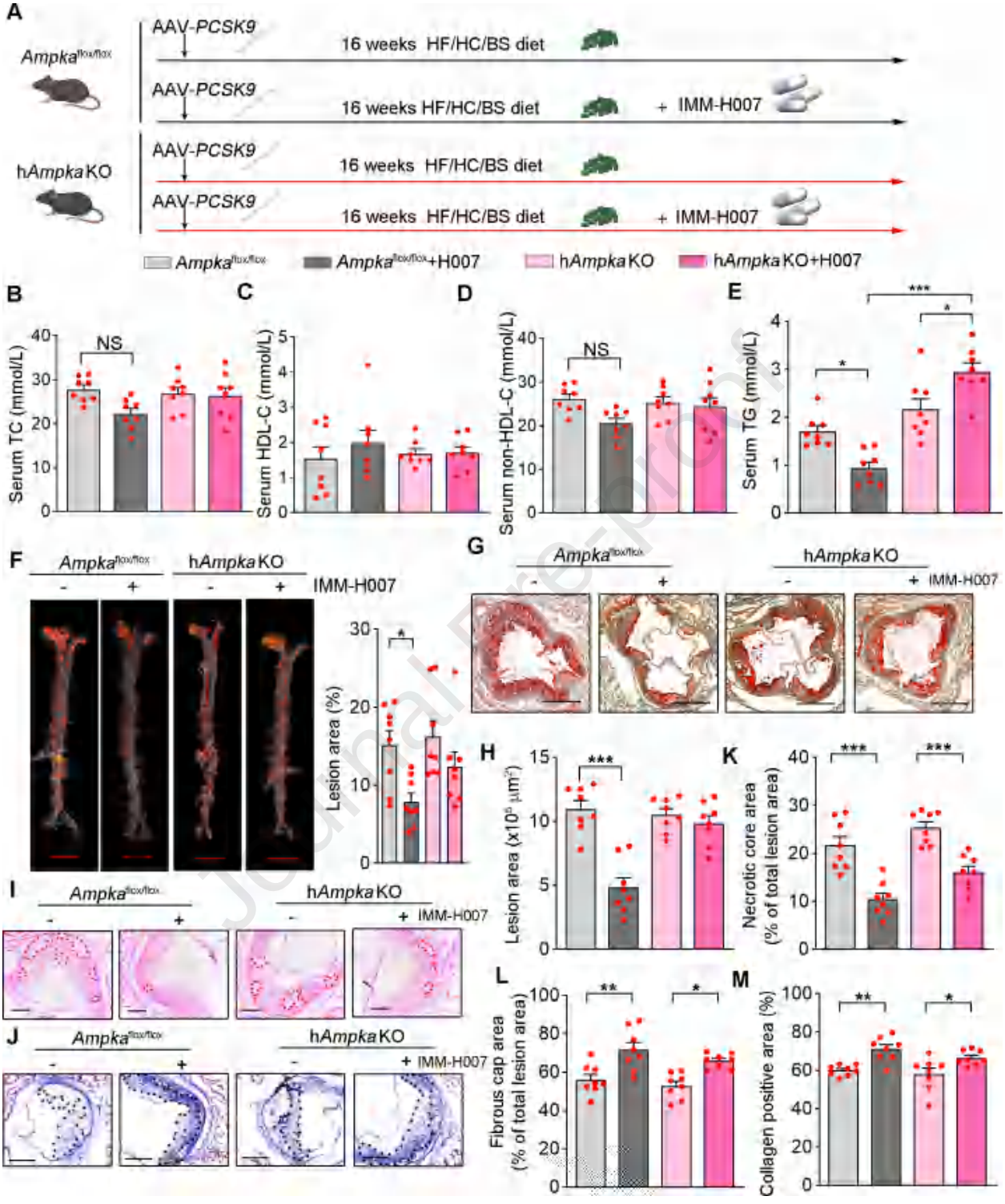
A
Ampka flox/flox
AAV-PCSK9
16 weeks HF/HC/BS diet
AAV-PCSK9
16 weeks HF/HC/BS diet
+ IMM-H007
hAmpkaKO
AAV-PCSK9
16 weeks HF/HC/BS diet
AAV-PCSK9
16 weeks HF/HC/BS diet
+ IMM-H007
Ampka flox/flox
Ampka flox/flox+H007
hAmpkaKO
hAmpkaKO+H007
B
Serum TC (mmol/L)
NS
C
Serum HDL-C (mmol/L)
D
Serum non-HDL-C (mmol/L)
NS
E
Serum TG (mmol/L)
F
Ampka flox/flox
hAmpkaKO
IMM-H007
Lesion area (%)
G
Ampka flox/flox
hAmpkaKO
IMM-H007
H
Lesion area (x10⁵ μm²)
K
Necrotic core area (% of total lesion area)
I
Ampka flox/flox
hAmpkaKO
IMM-H007
J
Ampka flox/flox
hAmpkaKO
IMM-H007
L
Fibrous cap area (% of total lesion area)
M
Collagen positive area (%)